AEDC-TR-78-49

c.2

Separated and Nonseparated Turbulent Flows about Axisymmetric Nozzle Afterbodies

Part I
Detailed Surface Measurements

John A. Benek
ARO, Inc.

October 1979

Final Report for Period October 1, 1976 – September 30, 1977

Approved for public release; distribution unlimited.

ARNOLD ENGINEERING DEVELOPMENT CENTER
ARNOLD AIR FORCE STATION, TENNESSEE
AIR FORCE SYSTEMS COMMAND
UNITED STATES AIR FORCE

NOTICES
When U. S. Government drawings, specifications, or other data are used for any purpose other than a definitely related Government procurement operation, the Government thereby incurs no responsibility nor any obligation whatsoever, and the fact that the Government may have formulated, furnished, or in any way supplied the said drawings, specifications, or other data, is not to be regarded by implication or otherwise, or in any manner licensing the holder or any other person or corporation, or conveying any rights or permission to manufacture, use, or sell any patented invention that may in any way be related thereto.
Qualified users may obtain copies of this report from the Defense Documentation Center.
References to named commerical products in this report are not to be considered in any sense as an indorsement of the product by the United States Air Force or the Government.

This report has been reviewed by the Information Office (OI) and is releasable to the National Technical Information Service (NTIS). At NTIS, it will be available to the general public, including foreign nations.

APPROVAL STATEMENT

This report has been reviewed and approved.

Elton R Thompson

ELTON R. THOMPSON
Project Manager
Directorate of Technology

Approved for publication:

FOR THE COMMANDER

Marion L. Laster

MARION L. LASTER
Director of Technology
Deputy for Operations

REPORT DOCUMENTATION PAGE		READ INSTRUCTIONS BEFORE COMPLETING FORM
1. REPORT NUMBER AEDC-TR-78-49	2. GOVT ACCESSION NO.	3. RECIPIENT'S CATALOG NUMBER
4. TITLE *(and Subtitle)* SEPARATED AND NONSEPARATED TURBULENT FLOWS ABOUT AXISYMMETRIC NOZZLE AFTERBODIES - PART I DETAILED SURFACE MEASUREMENTS		5. TYPE OF REPORT & PERIOD COVERED Final Report-October 1, 1976 - September 30, 1977 6. PERFORMING ORG. REPORT NUMBER
7. AUTHOR(s) John A. Benek, ARO, Inc., a Sverdrup Corporation Company		8. CONTRACT OR GRANT NUMBER(s)
9. PERFORMING ORGANIZATION NAME AND ADDRESS Arnold Engineering Development Center/DOT Air Force Systems Command Arnold Air Force Station, Tennessee 37389		10. PROGRAM ELEMENT, PROJECT, TASK AREA & WORK UNIT NUMBERS Program Element 65807F
11. CONTROLLING OFFICE NAME AND ADDRESS Arnold Engineering Development Center/DOS Arnold Air Force Station, Tennessee 37389		12. REPORT DATE October 1979 13. NUMBER OF PAGES 49
14. MONITORING AGENCY NAME & ADDRESS*(if different from Controlling Office)*		15. SECURITY CLASS. *(of this report)* UNCLASSIFIED 15a. DECLASSIFICATION/DOWNGRADING SCHEDULE N/A

16. DISTRIBUTION STATEMENT *(of this Report)*
Approved for public release; distribution unlimited.

17. DISTRIBUTION STATEMENT *(of the abstract entered in Block 20, if different from Report)*

18. SUPPLEMENTARY NOTES

Available in DDC

19. KEY WORDS *(Continue on reverse side if necessary and identify by block number)*

transonic flow	axisymmetric	Mach numbers
static pressure	circular arc	Reynolds numbers
boundary layer	models (boattail)	
flow	plumes	
testing	simulators	

20. ABSTRACT *(Continue on reverse side if necessary and identify by block number)*

Extensive static pressure data were obtained on a model consisting of a cone-ogive-cylinder forebody, two interchangeable circular arc afterbody boattails having length-to-forebody diameter ratios (ℓ/D) of 0.80 and 1.77, and two interchangeable solid exhaust plume simulators of cylindrical and contoured geometry. Boundary-layer pitot data and photographic records of model tufts and schlieren data were also obtained. Data were

DD FORM 1 JAN 73 1473 EDITION OF 1 NOV 65 IS OBSOLETE

20. ABSTRACT (Continued)

collected over a Mach number range of 0.60 to 1.30 and a unit Reynolds number range of 3.2 to 13.12 x 10^6/m (1 to 4 x 10^6/ft) at zero angle of attack and sideslip for the purpose of obtaining experimental data suitable for comparison with theoretical predictions. Data are presented for two model configurations with cylindrical solid plume simulators at three flow conditions: (1) ℓ/D = 1.77 boattail at Mach number 0.80 and Reynolds number 8.2 x 10^6/m for high subsonic, unseparated flow; (2) ℓ/D = 0.80 boattail at Mach number 0.60 and unit Reynolds number 8.2 x 10^6/m for subsonic, separated flow; and (3) ℓ/D = 0.80 boattail at Mach number 0.95 and unit Reynolds number 8.2 x 10^6/m for transonic, separated flow with boundary-layer-shock interaction.

AFSC
Arnold AFS Tenn

PREFACE

The work reported herein was conducted by the Arnold Engineering Development Center (AEDC), Air Force Systems Command (AFSC). The results of the investigation were obtained by ARO, Inc., AEDC Division (a Sverdrup Corporation Company), operating contractor for the AEDC, AFSC, Arnold Air Force Station, Tennessee, under ARO Project No. P41T-M1A in support of Research Project No. P32P-R4. Elton R. Thompson was the Air Force project manager. The data analysis was completed on September 1, 1977, and the manuscript was submitted for publication on July 25, 1978.

CONTENTS

ILLUSTRATIONS

Figure

Page

TABLES

1.0 INTRODUCTION

The dependence of overall aircraft performance upon the aft end drag is well known to the aircraft designer. Therefore, it is extremely desirable to acquire an accurate knowledge of the flow field over the nozzle afterbody (NAB) portion of the airframe. For this reason extensive experimental data of various NAB designs have been compiled, some of which attempt to account for the proper effects of the exhaust plume upon the flow field. To complement the experimental studies, a large effort has been undertaken to develop analytical tools to compute the flow field. However, the complexity of the flow field makes the development of any analytical effort an arduous task. This is because computations must properly account not only for the influence of NAB geometry and the interaction between the exhaust plume and flow over the afterbody but also for the presence and extent of flow separation and, at transonic speeds and above, for shock-boundary layer interactions.

Before any analytical technique can be used with confidence, it must be verified by making careful comparisons with high-quality experimental data. The data should be acquired on a model of simple but representative geometry in a single experiment so that dependent variables can be carefully controlled. At the present time, there is an acute scarcity of experimental data meeting the above criteria, especially for the separated flow case. The work described herein initiates an effort directed at alleviating this deficiency.

In this series of experiments extensive pressure data were obtained on a large model, L = 4.8 m (15.8 ft), which consisted of a cone-ogive-cylinder forebody, two interchangeable circular arc boattail afterbodies (ℓ/D = 0.80 and 1.77), and two interchangeable solid plume simulators. The model thus provides four separate geometries and sufficient size to allow high spatial resolution of static pressure orifice locations and boundary-layer rake positions. In addition, photographic records of

model tufts and schlieren data were obtained on all four geometries. Data were acquired at zero angle of attack and sideslip over a Mach number range of $0.60 \leq M_\infty \leq 1.3$ and a unit Reynolds number range of $3.3 \times 10^6/m \leq Re_\infty \leq 13.2 \times 10^6/m$ ($1 \times 10^6/ft \leq Re_\infty \leq 4 \times 10^6$ ft).

Additional experimental data, Part II of this work, covering these nozzle afterbody configurations for Mach number 0.64 and a unit Reynolds number of 2.888×10^5 are contained in AEDC-TR-79-22.

2.0 APPARATUS

2.1 WIND TUNNEL

The AEDC Propulsion Wind Tunnel(16T) (Tunnel 16T) is a closed-circuit, continuous flow wind tunnel with an operational Mach number range of 0.2 to 1.60. The test section is 4.88 x 4.88 m (16 x 16 ft) in cross section and 12.2 m (40 ft) in length. The tunnel can be operated within a stagnation pressure range of 5.75×10^3 to 1.91×10^6 pascals (120 to 4,000 psfa) where the exact limits are Mach number dependent. The tunnel temperature can be varied between 27 to 71.5°C (80 to 160°F). Perforated walls (six-percent porosity) in the test section allow continuous operation through the Mach number range with a minimum of wall interference. Subsonic test section Mach numbers are obtained by setting tunnel total pressure and plenum static pressure, whereas supersonic Mach numbers are obtained by setting nozzle contour, tunnel total pressure, and plenum static pressure in accordance with a test section calibration. A more complete description of the wind tunnel and its operating characteristics can be found in Ref. 1. The perforated wall pattern and model location in the test section is shown in Fig. 1.

2.2 MODEL CONFIGURATION

The model was a sting-mounted body of revolution consisting of a cone-ogive-cylinder forebody, two interchangeable afterbodies, and two

interchangeable solid plume simulators. The cone nose had a 15-deg half-angle, a 6-mm (0.24 in.) spherical tip, and a tangent-ogive shoulder to provide a smooth geometrical transition to the cylindrical portion of the forebody (see Fig. 2). The afterbody boattails were circular arc sections with a length-to-maximum body diameter ratio (ℓ/D) of 0.80 and 1.77. Both boattail arcs were tangent to the cylindrical forebody at model station (MS) 331.39 cm as shown in Fig. 2. The plume simulators were (1) a cylindrical plume with a constant 12.78-cm (5.03 in.) diameter and (2) a contoured plume which varied smoothly from 12.78- to 17.09-cm (6.728 in.) diameter in an axial distance of 15.74 cm (6.197 in.). The contour was then continued downstream at a constant 17.09-cm diameter. This contour is similar to an actual exhaust plume geometry operating at a nozzle pressure ratio (nozzle exit static pressure ratioed to the free-stream static pressure) of approximately 4.7. The interchangeable afterbodies and solid plume simulators together provided four separate model configurations. These configurations were designated as follows:

Configuration Designation No.	Model	
	Boattail (ℓ/D)	Plume Type
1	1.77	Cylindrical
2	1.77	Contoured
3	0.80	Cylindrical
4	0.80	Contoured

Model Configuration No. 1 is shown in Fig. 3. The model was sting mounted to eliminate strut interference problems and to facilitate model changes. The pertinent dimensions of the afterbodies are illustrated in Fig. 4, and similar illustrations of the solid plume simulators are shown in Fig. 5. A complete summary of geometrical coordinates (MS,r) for each configuration is given in Table 1. Model axial locations, designated MS, are referenced to a point 1.83 cm (0.72 in.) ahead of the

physical origin of the model. This point corresponds to the origin of the 15-deg conical section of the forebody. The tabulated radial coordinate at each axial location is an average value of four to eight separate measurements of the radius at equal increments around the model circumference.

2.3 INSTRUMENTATION

Approximately 200 static pressure orifices were distributed along the top of the model (oriented to face the upper wall of the tunnel test section). The orifices were spaced at 1.27-cm (0.5 in.) intervals along the cone-ogive portion of the forebody, the afterbodies, and the plume simulators, and at 15.24-cm (6.0 in.) intervals along the cylindrical portion of the forebody. The exact number of static pressures varied between model configurations because of the difference in lengths of the afterbodies and plume simulators. In addition, each configuration was equipped with five boundary-layer rakes having ten pitot probes each for a total of 50 pitot pressures. The pitot probes were made from 1.63-mm (0.064 in.) -OD tubing having a 0.29-mm (0.0095 in.) wall. The boundary-layer rakes were spaced radially around the model circumference in the angular segment between 120 deg and 210 deg as measured from the position of the static orifices (see Fig. 3). The sketches of Fig. 6 illustrate the arrangement of the boundary-layer rakes. All model pressures were measured by six 48-port Scanivalves®.

Electrical signals from the Scanivalves and standard tunnel instrumentation were digitized and input directly to the facility computer for online data reduction. The model static pressure data were also monitored graphically on a cathode ray tube (CRT) plotter during the course of the experiment.

Tufts were located about the model circumference at 30-deg intervals in a region extending roughly one meter on either side of the boattail-

plume junction. The tufts were made from 0.03-mm (0.0012 in.) -nominal-diam nylon monofilament of approximately 2.5-cm (1 in.) length. They were affixed to the model by a drop of epoxy cement which formed a small raised spot approximately 0.03 mm (0.0012 in.) in height and 6 mm (0.24 in.) in diameter. The tufts were made highly visible by dyeing the monofilament with an ultraviolet dye and then utilizing black light for illumination.* Tuft behavior under flow conditions was photographically recorded by both still and motion-picture cameras located in the tunnel top and sidewalls. Schlieren data were similarly recorded from the sidewall view for each flow condition.

3.0 PROCEDURE

3.1 FACTORS AFFECTING THE DATA

A boundary-layer trip located at MS 27.2 consisted of 3.2-mm (0.125 in.) -diam spheres tack welded to a 0.76-mm (0.003 in.) -thick by 12.7-mm (0.5 in.) -wide shim stock strip at a spacing of approximately four sphere-diameters. Runs made with and without the trip indicated no measurable difference in either the static pressure distributions or the boundary-layer profiles in the region of primary interest, i.e., MS = 250 to 380.

Runs made without the first three boundary-layer rakes (PT1XX, PT2XX, and PT3XX, see Fig. 6) indicated that the data from the fifth rake (PT5XX) were influenced by the first rake (PT1XX). Therefore, only data from the first four boundary-layer rakes, i.e., PT1XX through PT4XX, are presented in this report.

---

*This technique was developed by Crowder of the McDonnell Douglas Corporation (see Ref. 2 for details).

During the course of fabrication of the $\ell/D = 1.77$ afterbody boattail, the model was inadvertently damaged. This necessitated a change in the boattail contour from the designed circular arc. Additionally, model assembly required some fitting which resulted in a small but significant surface irregularity in the vicinity of the static pressure orifices between MS = 334.6 and 338.4 (131.7 and 133.2 in.). Therefore, the measured pressure distribution in this region cannot be expected to be entirely representative of an $\ell/D = 1.77$ circular arc boattail. These geometric irregularities are represented in Table 1.

The model blockage for these experiments was small, 0.21 percent. Therefore, no attempt was made to assess wall interference effects on these experimental data.

3.2 DATA REDUCTION

The standard data reduction program for Tunnel 16T was utilized to define free-stream properties. The measured pressures were converted to coefficient form:

$$CP(MS) = \frac{PS(MS) - P_\infty}{q_\infty}$$

where PS(MS) is the local static, P_∞ is the free-stream static, and q_∞ is the free-stream dynamic pressure. The boundary-layer data were reduced according to the procedures given in Ref. 3.

3.3 EXPERIMENTAL PROCEDURE

When test conditions were established, the pressure data and standard tunnel operating parameters were automatically recorded and reduced. An online output of these data were monitored from the standard computer output, as well as on a CRT plotter. Schlieren and tuft data were photographically recorded by both still and motion-picture cameras.

Tunnel operating parameters were also recorded during the photographic data acquisition. During the course of the test, free-stream conditions were virtually identical for duplicated test conditions.

3.4 UNCERTAINTY OF MEASUREMENTS

The estimated uncertainty of measurements (a combination of systematic and random error) in wind tunnel total, static, and dynamic pressures for several points in the test matrix are presented in Table 3. Scanivalve measurement uncertainties were also combined with tunnel parameter uncertainties, assuming a Taylor series method of error propagation, to estimate uncertainties in the final reduced pressures. Resultant values of the maximum expected uncertainty in CP = 0, i.e., PS = P_∞, are included in Table 3.

4.0 RESULTS AND DISCUSSION

4.1 GENERAL

Data were obtained at free-stream Mach numbers of 0.60, 0.70, 0.80, 0.85, 0.90, 0.95, 1.10, 1.20, and 1.30 at unit Reynolds numbers of 3.28 x 10^6, 8.20 x 10^6, 11.48 x 10^6, and 13.12 x 10^6/m (1 x 10^6, 2.5 x 10^6, 3.5 x 10^6, and 4 x 10^6/ft). Table 2 gives a summary of the complete test matrix covered. Because of the amount of data acquired, only data at unit Reynolds numbers of Re_∞ 8.2 x 10^6/m and M_∞ = 0.80 for Configuration No. 1 and M_∞ = 0.60 and 0.95 for Configuration No. 3 are presented in detail in this report. These data were chosen because they represent, respectively, high subsonic, attached flow; subsonic, separated flow; and transonic, separated flow with shock-boundary-layer interaction. These represent data from conditions suitable for initial comparisons with developmental computational techniques. The interested investigator may obtain a complete set of data summarized in Table 2 by contacting the Air Force project manager (see Preface).

4.2 EFFECT OF BOUNDARY-LAYER TRIP

The model boundary layer was tripped by means of a trip ring located at MS 27.23 (10.72 in.). Because the trip was large compared to the boundary-layer thickness at this location, it was deemed necessary to ascertain the influence of the trip on the boattail pressure distribution. Figure 7 presents a comparison of the axial pressure coefficients in the region of the boattail with and without the trip. This is typical of data obtained with and without the trip across the entire test matrix with this model configuration. Therefore, it was concluded that the trip did not adversely affect the data, and all other data were obtained with the trip ring in position.

4.3 PRESSURE DISTRIBUTIONS

The data corresponding to Configuration No. 1 at $M_\infty = 0.8$ and $Re_\infty = 8.2 \times 10^6$/m ($2.5 \times 10^6$/ft) and to Configuration No. 3 at $M_\infty = 0.6$ and 0.95 at $Re_\infty = 8.2 \times 10^6$/m are presented in tabular form in Table 4. The data include the axial location of the static pressure orifice in meters and the corresponding pressure coefficient, CP, for a given Mach number, M_∞, and unit Reynolds number, Re_∞, per meter. Following the static pressure data are the boundary-layer rake data for each of the first four total-pressure rakes (see Fig. 6). These data include the probe designation, the probe height measured perpendicular to the body at the probe location (in meters), and the corresponding value of pressure (in pascals). For each data set the value of total pressure, PT (pascals), free-stream static pressure, PS (pascals), and free-stream static temperature, TS (°K) are presented.

A visual summary of the static pressure data is shown by Figs. 8 through 10 where CP is given as a function of the dimensionless axial length parameter $\bar{X} = (MS-331.39)/D$, i.e., the distance in body diameters upstream and downstream from the forebody-boattail junction. The

rather large scatter of the data near $\bar{X} = 0$ in Fig. 8 is attributed to the geometric irregularity of this region as noted in Section 3.2.

The boundary-layer integral parameters corresponding to the pitot profiles of Table 4 are presented in Table 5. Table 5 gives the axial location of the pitot probe, the displacement thickness, δ^*, the momentum thickness, θ, the local skin friction coefficient, c_f, and the Reynolds number based upon the local boundary-layer edge conditions and the momentum thickness, R_θ. The data of Table 5 were computed by a standard boundary-layer data reduction program described in Ref. 3. Profiles which are judged to be separated are indicated by an S.

4.4 FLOW VISUALIZATION

Photographs were taken of the tufts at each run condition by illuminating the model with ultraviolet light. The tufts then became fluorescent and highly visible against the darkened background. One unexpected result was the loss of the tufts whenever a sufficiently violent separation was incurred. This situation generally resulted when a shock wave formed on the boattail and induced separation. Under these conditions the tufts fluctuated violently and broke off at the point where they were affixed to the model surface.

As a result of the loss of tufts from the model surface, only a limited amount of this type of data can be considered to provide useful information. Those data which are deemed to have value are indicated in Table 2 by a T. In fact, no data are available for Configuration No. 4 because of insufficient time to replace the extensive tuft loss encountered on Configuration No. 3. Similarly, the useful schlieren data are indicated in Table 2 by an S.

Photographic records of the orientation of the tufts for $Re_\infty = 8.2 \times 10^6$/m ($2.5 \times 10^6$/ft) and $M_\infty = 0.80$ for model Configuration No. 1 are

shown in Fig. 11. Similar records are shown for Configuration No. 3 at M_∞ = 0.60 and 0.95 in Fig. 12. Figure 12b for the M_∞ = 0.95 case has been included to illustrate typical records where the tufts were lost from the model surface. Schlieren photographs for Configuration No. 3 are presented in Fig. 13 for Re_∞ = 8.2 x 10^6/m (2.5 x 10^6/ft) and M_∞ = 0.60 and 0.95.

5.0 CONCLUDING REMARKS

Static pressure distributions, boundary-layer pitot pressures, and tuft and schlieren photographic data have been obtained from four combinations of two circular arc afterbody boattails (length-to-diameter ratios of 0.80 and 1.77) and two solid plume simulators (cylindrical and contoured geometries). These data were acquired with the principal objective of providing high-quality aerodynamic data which may be used as a standard for comparison with theoretical predictions. In particular, data were obtained at zero angle of attack and sideslip over a Mach number range of 0.60 to 1.30 and a unit Reynolds number range of 3.28 x 10^6/m (1 x 10^6/ft) to 13.12 x 10^6/m (4 x 10^6/ft). The shorter boattail afterbody provides an easily modeled geometry with separated flow over the entire test matrix.

Three sets of data are presented in detail in this report. These are: (1) long boattail with cylindrical plume at Mach number 0.80 (high subsonic unseparated flow), (2) short boattail with cylindrical plume at Mach number 0.60 (subsonic separated flow), and (3) short boattail with cylindrical plume at Mach number 0.95 (transonic separated flow with shock-boundary-layer interaction). All of these data have a unit Reynolds number of 8.2 x 10^6/m (2.5 x 10^6/ft).

The data were analyzed to determine their accuracy. As a result, it was determined that the boundary-layer trip on the model nose did not influence the measurements. However, the pitot data from the fifth

boundary-layer rake, PT5XX (Fig. 6), were found to be influenced by the wake of the first boundary-layer rake, PT1XX. Consequently, these data were excluded from consideration. Geometric irregularities in the ℓ/D = 1.77 circular arc boattail affected the model static pressure distribution between MS = 334.6 and 338.4. Finally, no attempt was made to assess the wall interference effects on these data.

REFERENCES

1. Test Facilities Handbook (Tenth Edition). "Propulsion Wind Tunnel Facility, Vol. 4." Arnold Engineering Development Center, May 1974.

2. Crowder, J. P. "Fluorescent Mini-Tufts for Non-Intrusive Flow Visualization." Report No. J7374, McDonnell Douglas Corporation, Douglas Aircraft Company.

3. Benek, John A. "Effects of Acoustic and Vortical Disturbances on the Turbulent Boundary Layer at Free-Stream Mach Number 0.5." AEDC-TR-77-73 (AD047921), Arnold Engineering Development Center, December 1977.

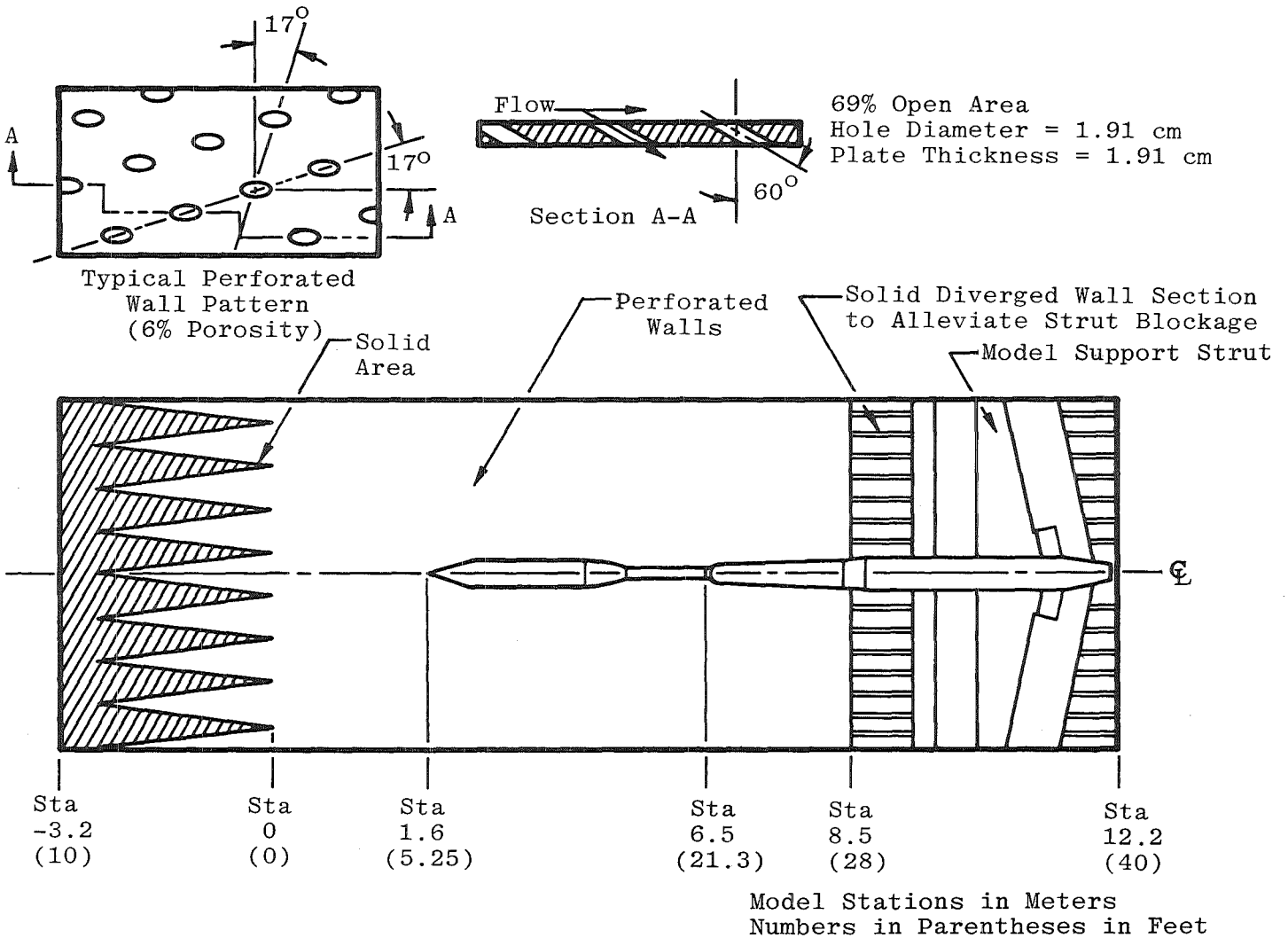

Figure 1. Location of model in wind tunnel test section.

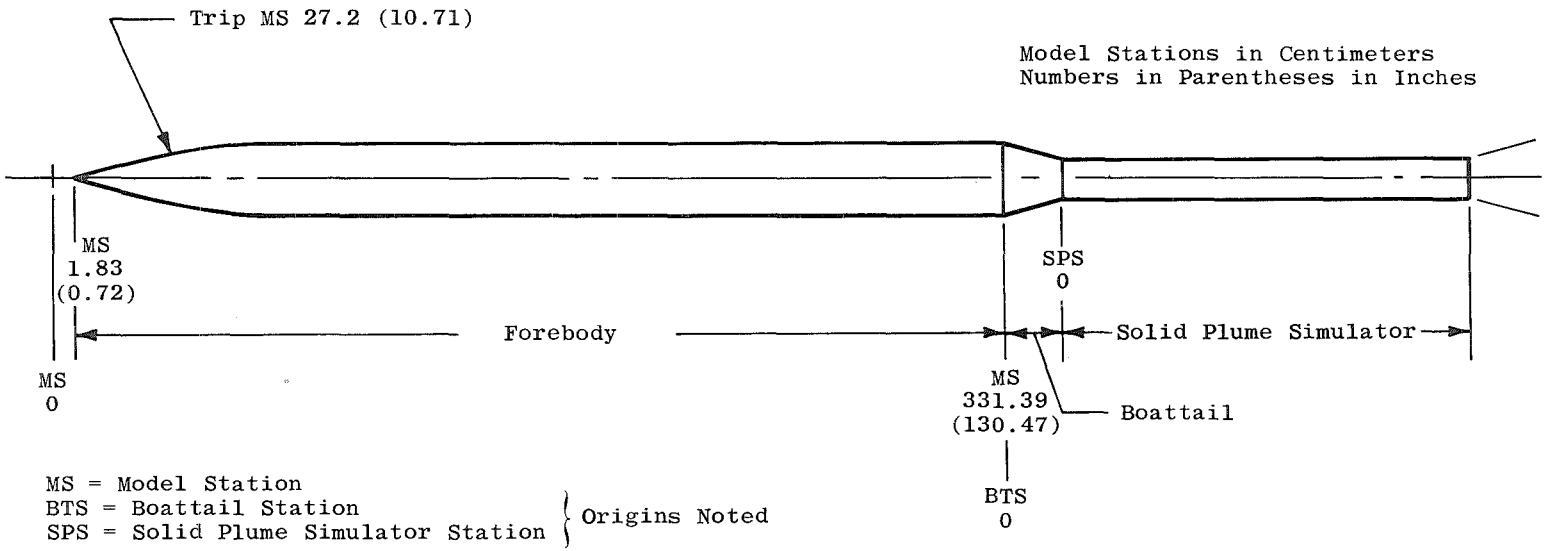

Figure 2. Details of model.

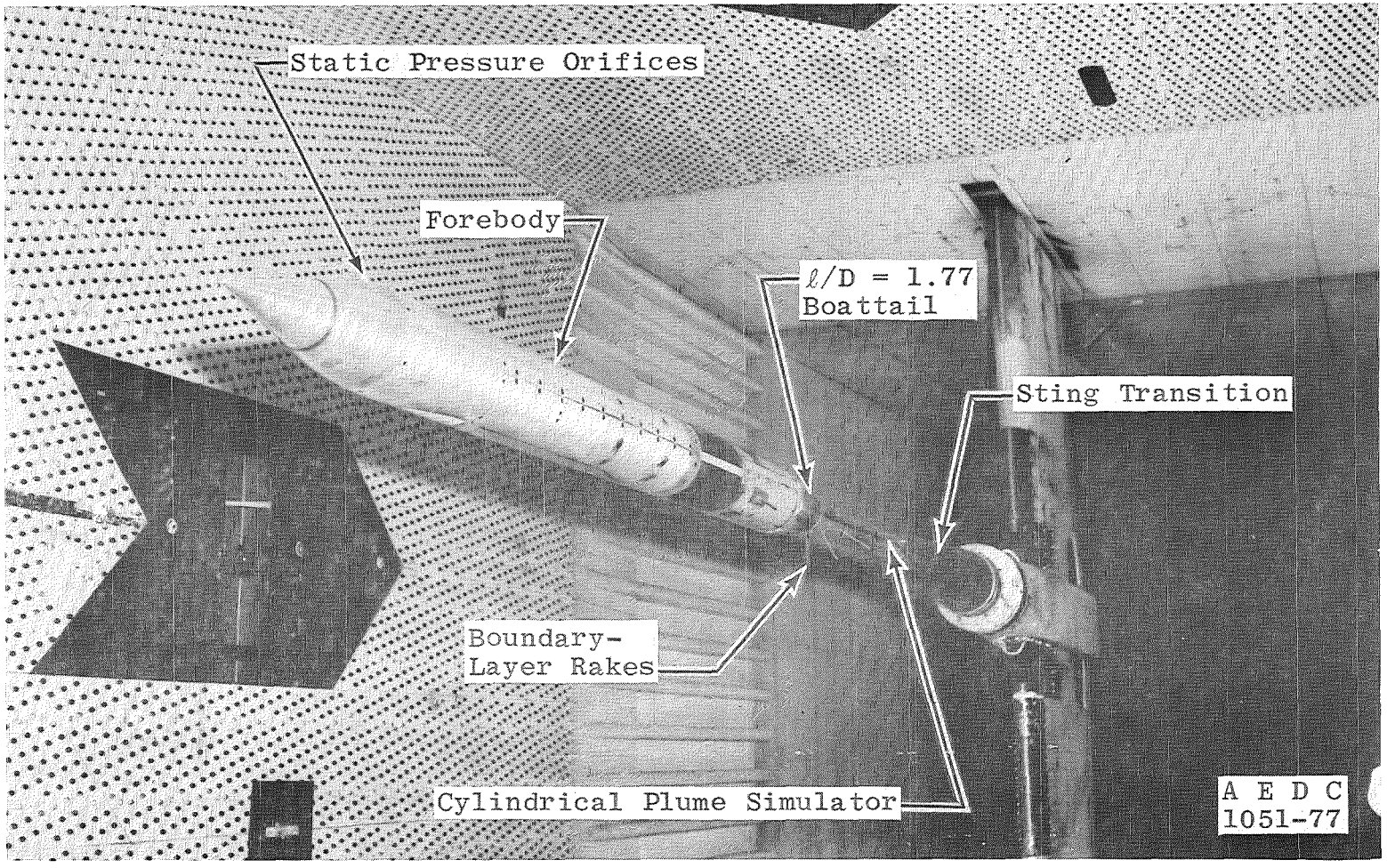

Figure 3. Installation photograph of model in test section.

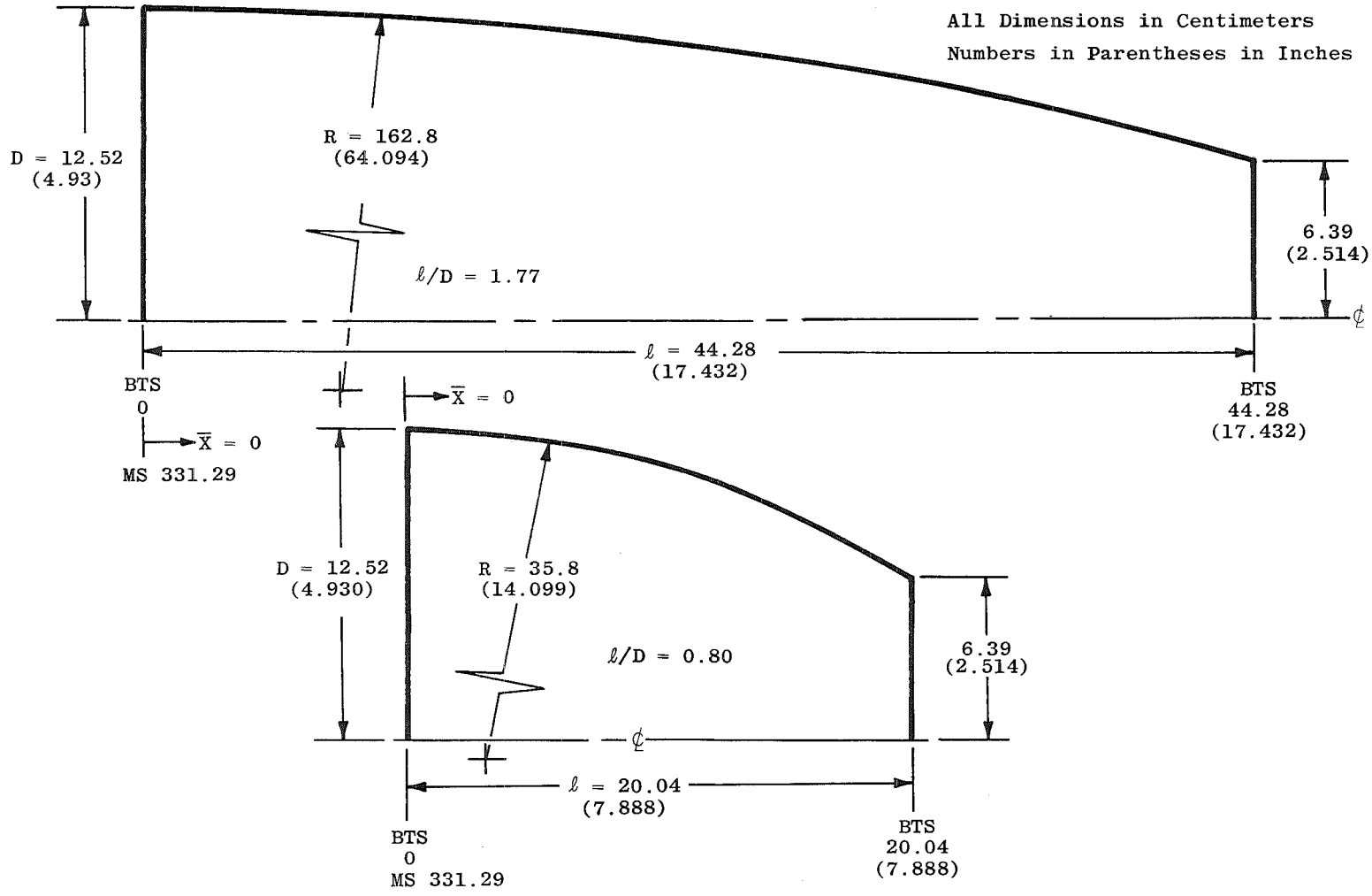

Figure 4. Boattail geometries.

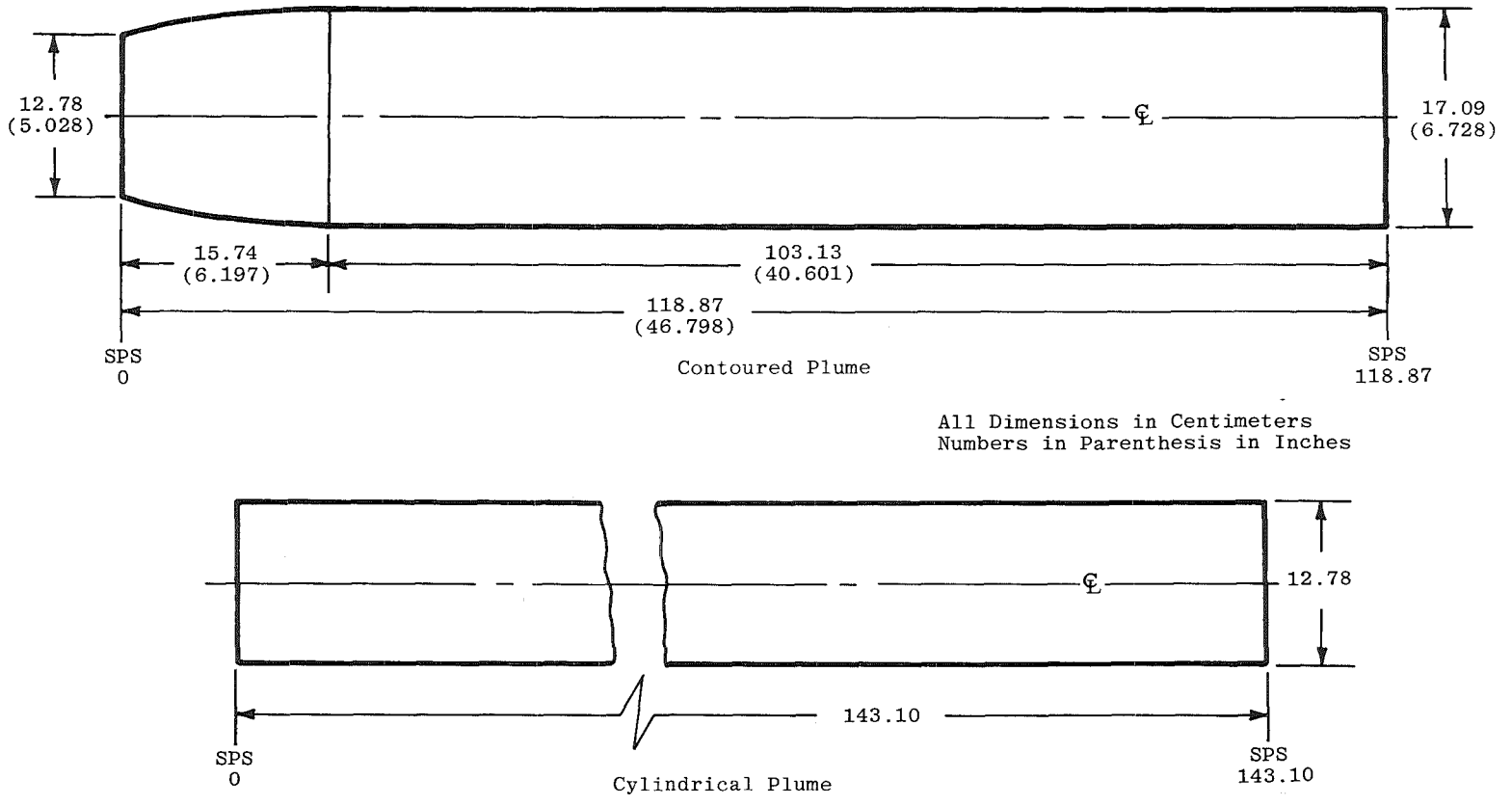

Figure 5. Solid plume simulator geometries.

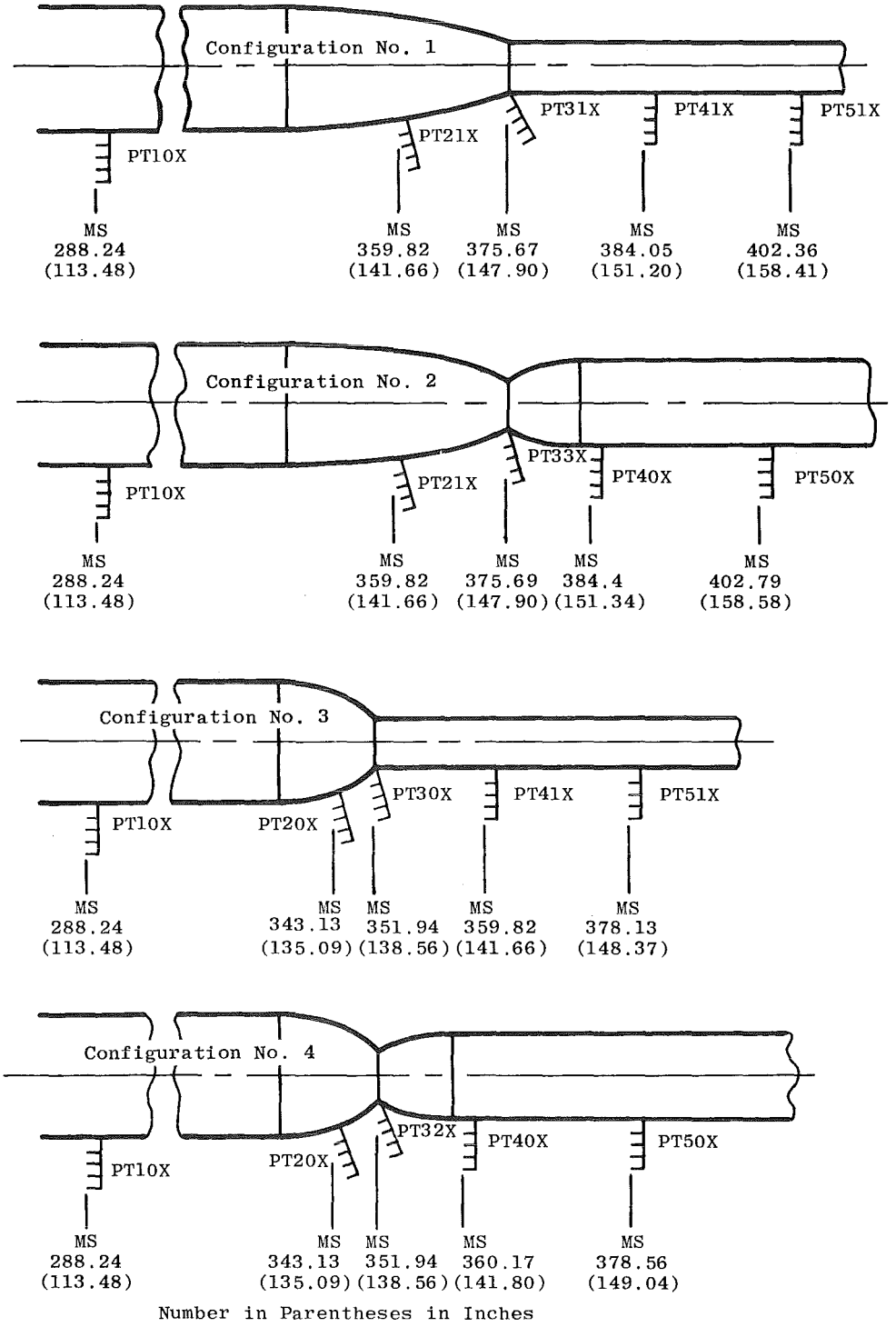

a. Axial locations

Figure 6. Total-pressure rake locations and designations.

Note: Rake tube spacings are defined with the pressure data in Table 4.

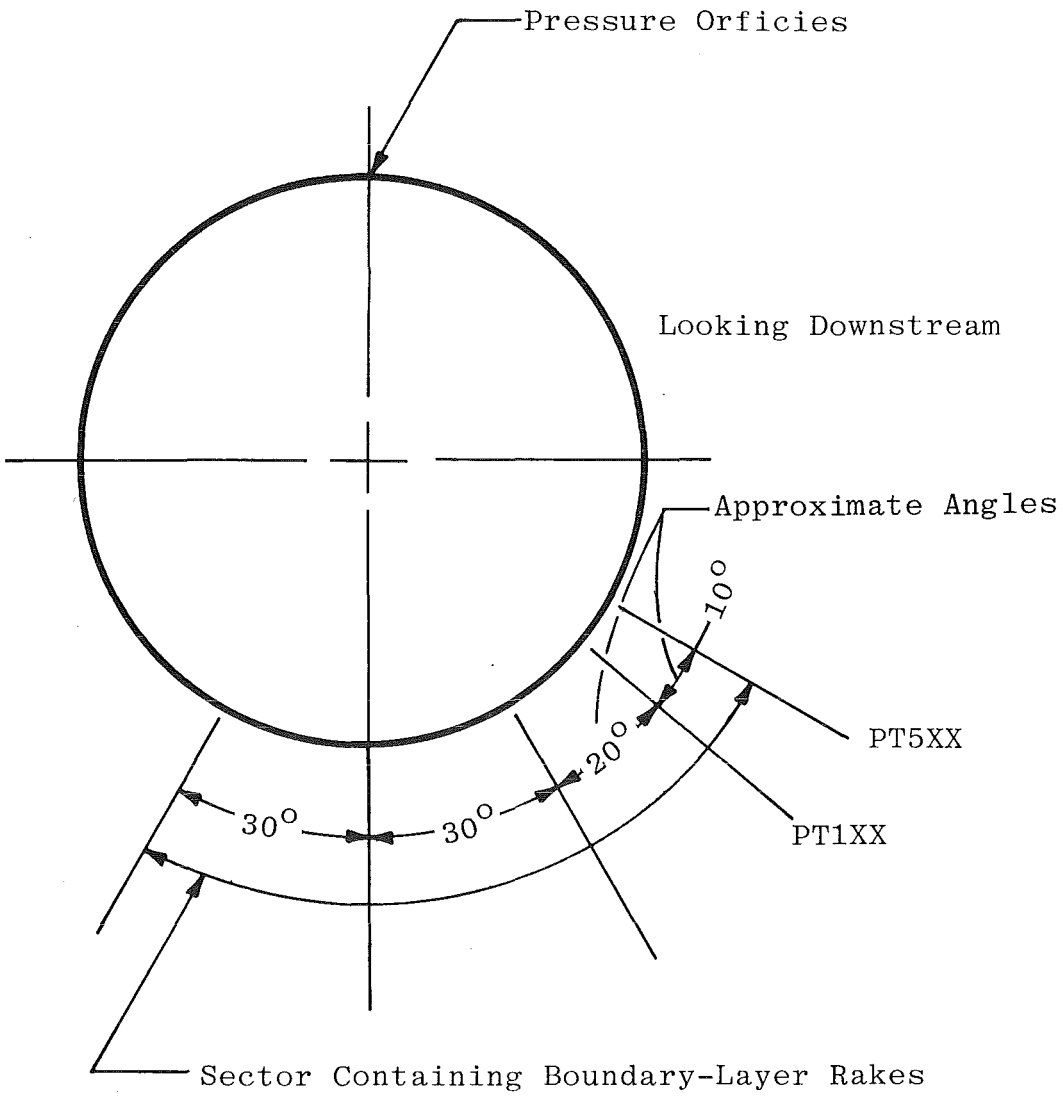

b. Circumferential boundary-layer rake positions
Figure 6. Concluded.

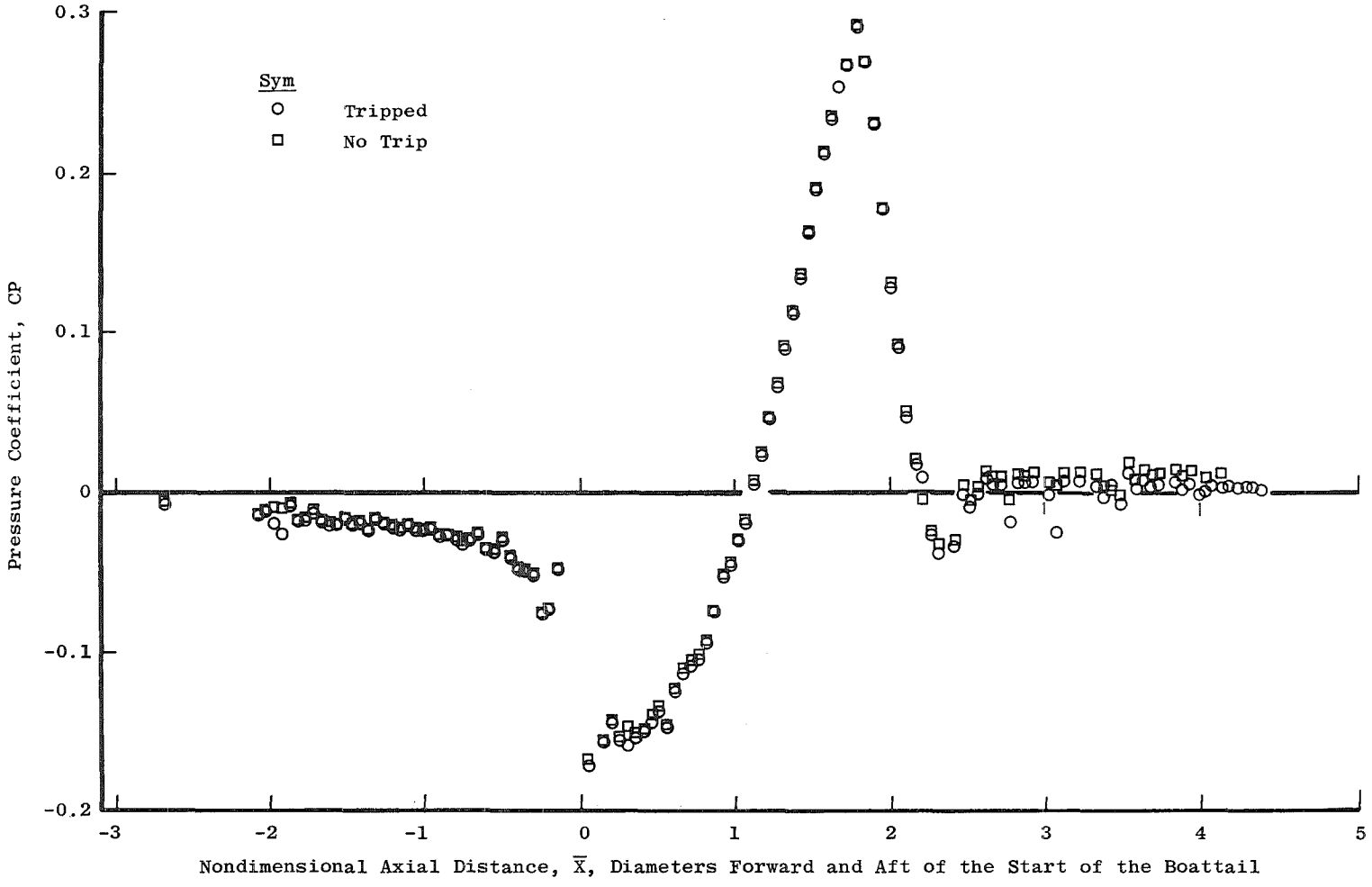

Figure 7. Effect of boundary-layer trip on pressure distribution, $M_\infty = 0.8$ and $Re_\infty = 8.2 \times 10^6$/m ($2.5 \times 10^6$/ft), configuration No. 2.

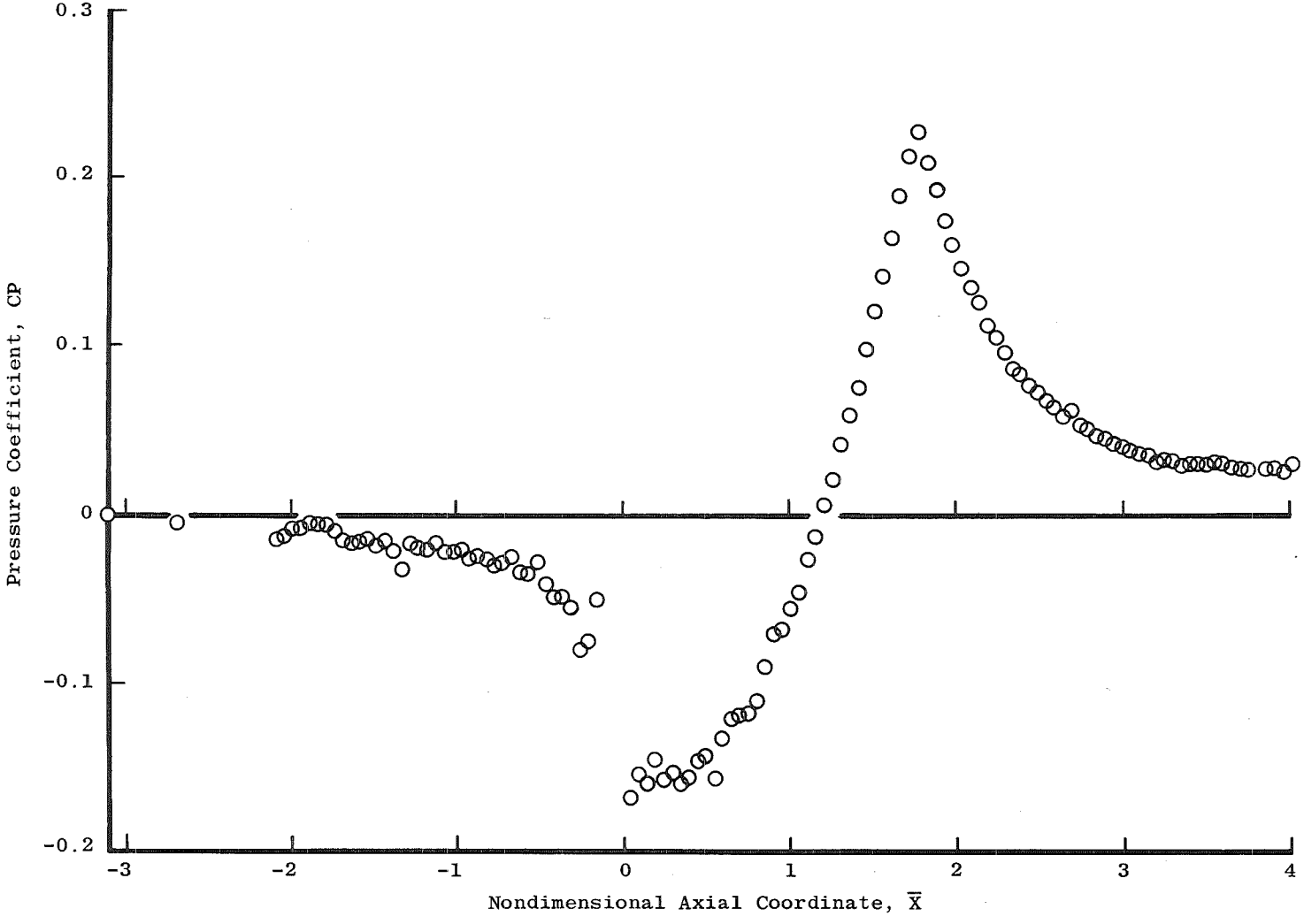

Figure 8. Pressure distribution for an unseparated case: configuration No. 1 at M_∞ = 0.80 and Re_∞ = 8.2 x 10^6/m (2.5 x 10^6/ft).

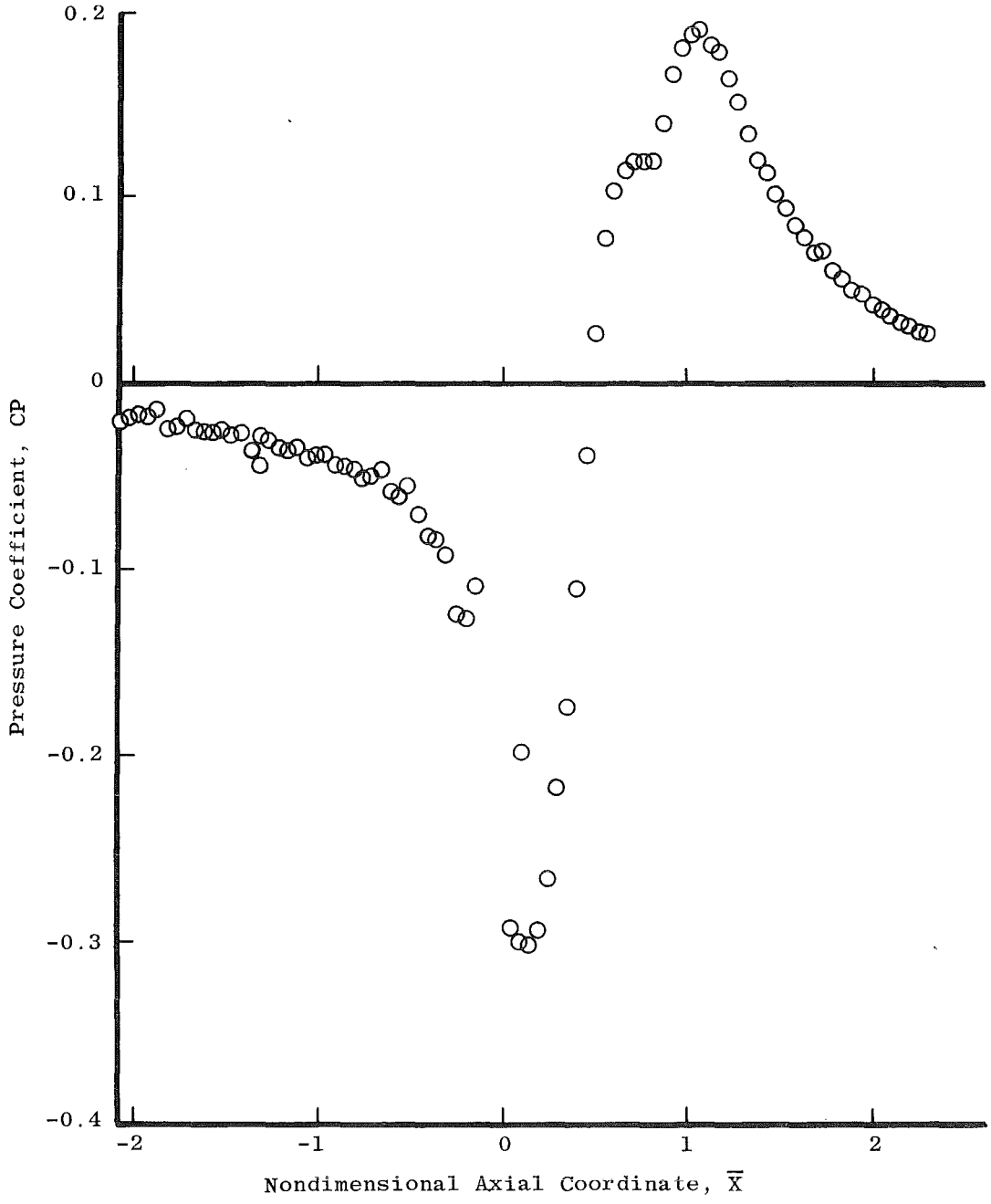

Figure 9. Pressure distribution for a subsonic separated case: configuration No. 3 at M_∞ = 0.60 and Re_∞ = 8.2 x 10^6/m (2.5 x 10^6/ft).

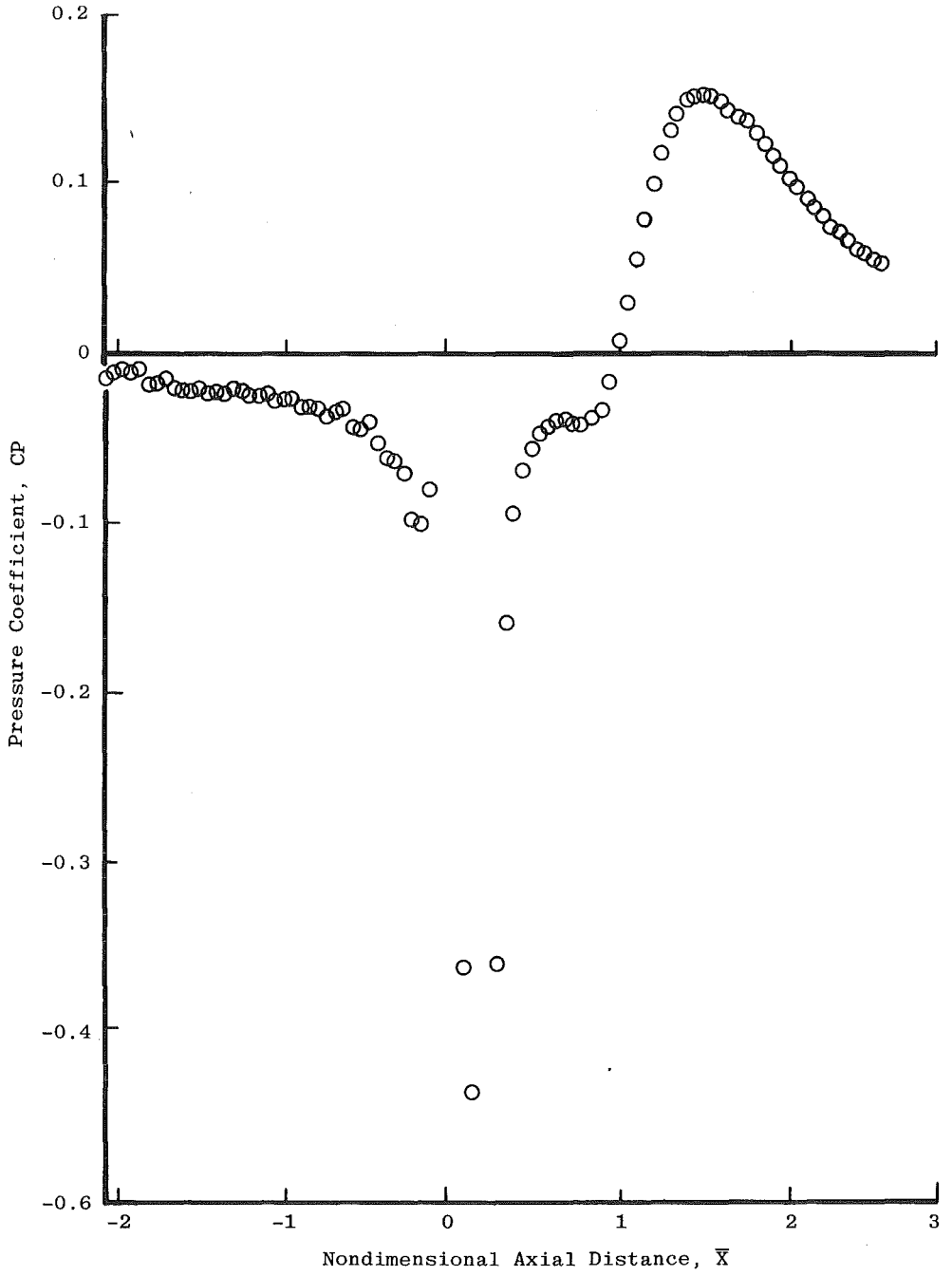

Figure 10. Pressure distribution for a transonic separated case: configuration No. 3 at M_∞ = 0.95 and Re_∞ = 8.2 x 10^6/m (2.5 x 10^6/ft).

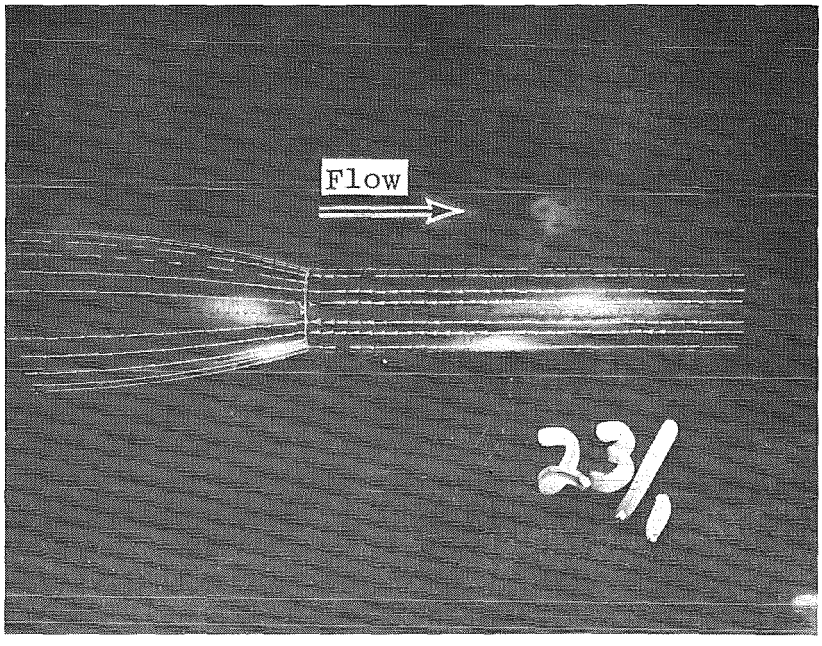

Note: Model boundary is closely approximated by the outermost rows of tufts.

Figure 11. Model configuration No. 1, tuft orientation.

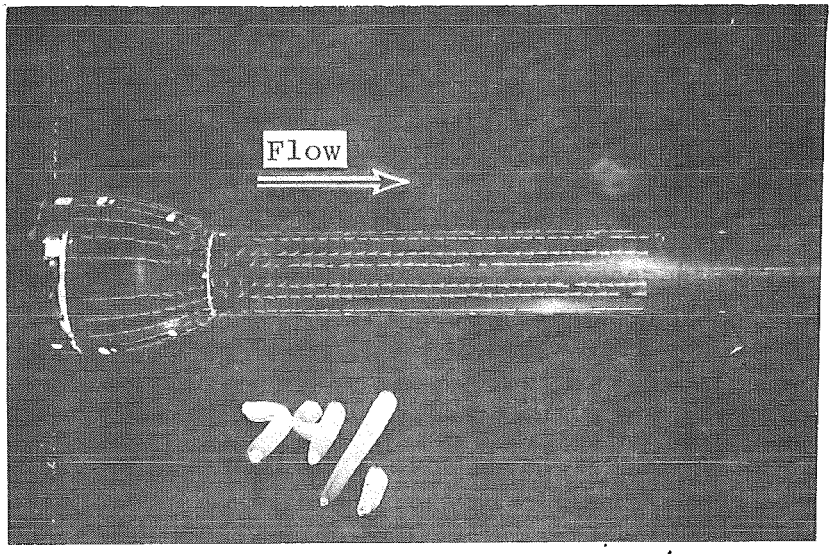

a. M_∞ = 0.60 and Re_∞ = 8.2 x 10^6/m (2.5 x 10^6/ft)

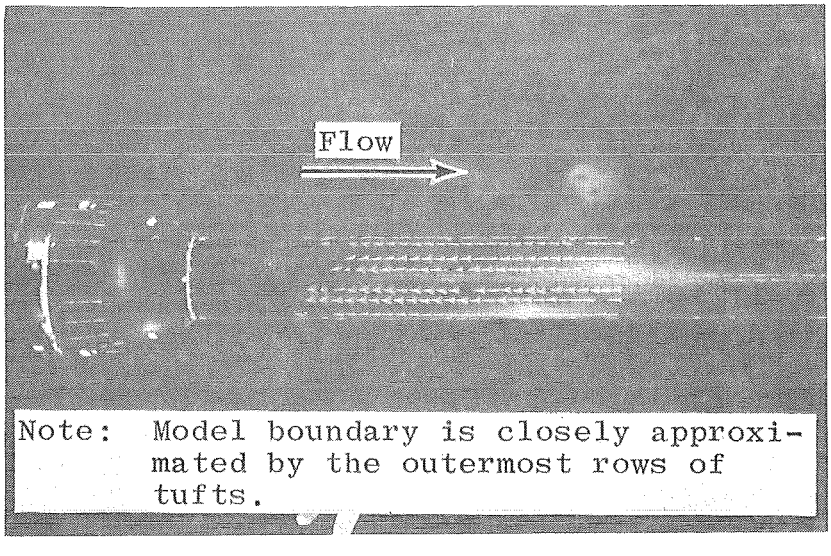

b. M_∞ = 0.95 and Re_∞ = 8.2 x 10^6/m (2.5 x 10^6/ft)

Figure 12. Model configuration No. 3, tuft orientation.

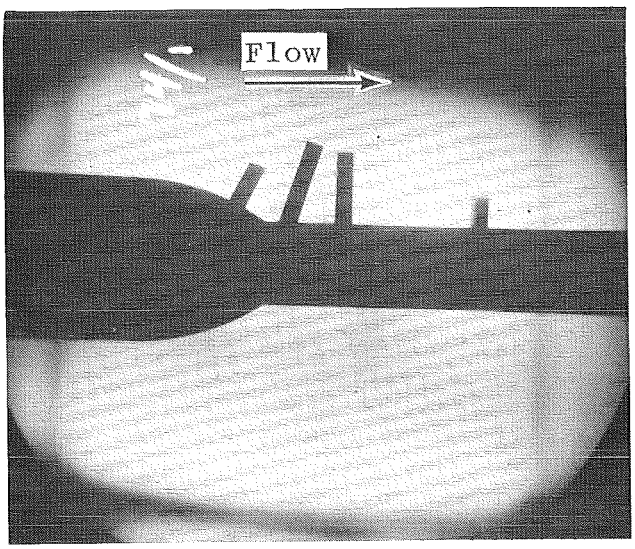

a. M_∞ = 0.60 and Re_∞ = 8.2 x 10^6/m (2.5 x 10^6/ft)

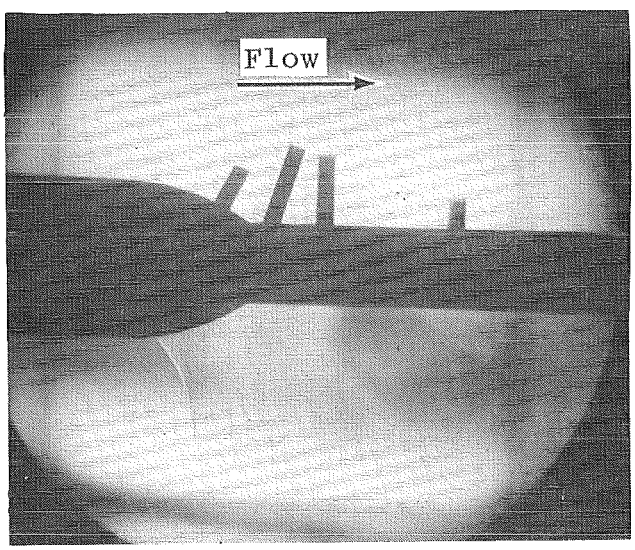

b. M_∞ = 0.95 and Re_∞ = 8.2 x 10^6/m (2.5 x 10^6/ft)

Figure 13. Schlieren photographs of model configuration No. 3.

Table 1. Model Geometries

Axial Position = MS, metric Local Model Radius = r, meters

Configuration No. 1		Configuration No. 2		Configuration No. 3		Configuration No. 4	
AXIAL POSITION	RADIUS	AXIAL POSITION	RADIUS	AXIAL POSITION	RADIUS	AXIAL POSITION	RADIUS
0.02540	0.00665	0.02540	0.00665	0.02540	0.00665	0.02540	0.00665
0.03810	0.00988	0.03810	0.00988	0.03810	0.00988	0.03810	0.00988
0.05080	0.01307	0.05080	0.01307	0.05080	0.01307	0.05080	0.01307
0.06350	0.01626	0.06350	0.01626	0.06350	0.01626	0.06350	0.01626
0.07620	0.01946	0.07620	0.01946	0.07620	0.01946	0.07620	0.01946
0.08890	0.02268	0.08890	0.02268	0.08890	0.02268	0.08890	0.02268
0.10160	0.02590	0.10160	0.02590	0.10160	0.02590	0.10160	0.02590
0.11430	0.02914	0.11430	0.02914	0.11430	0.02914	0.11430	0.02914
0.12700	0.03238	0.12700	0.03238	0.12700	0.03238	0.12700	0.03238
0.13970	0.03563	0.13970	0.03563	0.13970	0.03563	0.13970	0.03563
0.15240	0.03886	0.15240	0.03886	0.15240	0.03886	0.15240	0.03886
0.16510	0.04207	0.16510	0.04207	0.16510	0.04207	0.16510	0.04207
0.17780	0.04525	0.17780	0.04525	0.17780	0.04525	0.17780	0.04525
0.19050	0.04841	0.19050	0.04841	0.19050	0.04841	0.19050	0.04841
0.20320	0.05156	0.20320	0.05156	0.20320	0.05156	0.20320	0.05156
0.21590	0.05472	0.21590	0.05472	0.21590	0.05472	0.21590	0.05472
0.22860	0.05790	0.22860	0.05790	0.22860	0.05790	0.22860	0.05790
0.24130	0.06108	0.24130	0.06108	0.24130	0.06108	0.24130	0.06108
0.25400	0.06427	0.25400	0.06427	0.25400	0.06427	0.25400	0.06427
0.26670	0.06751	0.26670	0.06751	0.26670	0.06751	0.26670	0.06751
0.27940	0.07074	0.27940	0.07074	0.27940	0.07074	0.27940	0.07074
0.29210	0.07400	0.29210	0.07400	0.29210	0.07400	0.29210	0.07400
0.30480	0.07767	0.30480	0.07767	0.30480	0.07767	0.30480	0.07767
0.31750	0.08047	0.31750	0.08047	0.31750	0.08047	0.31750	0.08047
0.33020	0.08368	0.33020	0.08368	0.33020	0.08368	0.33020	0.08368
0.34290	0.08686	0.34290	0.08686	0.34290	0.08686	0.34290	0.08686
0.35560	0.09000	0.35560	0.09000	0.35560	0.09000	0.35560	0.09000
0.36830	0.09312	0.36830	0.09312	0.36830	0.09312	0.36830	0.09312
0.38100	0.09618	0.38100	0.09618	0.38100	0.09618	0.38100	0.09618
0.39370	0.09914	0.39370	0.09914	0.39370	0.09914	0.39370	0.09914
0.40640	0.10193	0.40640	0.10193	0.40640	0.10193	0.40640	0.10193
0.41910	0.10450	0.41910	0.10450	0.41910	0.10450	0.41910	0.10450
0.43180	0.10689	0.43180	0.10689	0.43180	0.10689	0.43180	0.10689
0.44450	0.10908	0.44450	0.10908	0.44450	0.10908	0.44450	0.10908
0.45720	0.11109	0.45720	0.11109	0.45720	0.11109	0.45720	0.11109
0.46990	0.11292	0.46990	0.11292	0.46990	0.11292	0.46990	0.11292
0.48260	0.11458	0.48260	0.11458	0.48260	0.11458	0.48260	0.11458
0.49530	0.11608	0.49530	0.11608	0.49530	0.11608	0.49530	0.11608
0.50800	0.11741	0.50800	0.11741	0.50800	0.11741	0.50800	0.11741
0.52070	0.11861	0.52070	0.11861	0.52070	0.11861	0.52070	0.11861
0.53340	0.11978	0.53340	0.11978	0.53340	0.11978	0.53340	0.11978
0.54610	0.12076	0.54610	0.12076	0.54610	0.12076	0.54610	0.12076
0.55880	0.12166	0.55880	0.12166	0.55880	0.12166	0.55880	0.12166
0.57150	0.12241	0.57150	0.12241	0.57150	0.12241	0.57150	0.12241
0.58420	0.12298	0.58420	0.12298	0.58420	0.12298	0.58420	0.12298
0.59690	0.12345	0.59690	0.12345	0.59690	0.12345	0.59690	0.12345

Table 1. Continued

Axial Position = MS, metric Local Model Radius = r, meters

Configuration No. 1		Configuration No. 2		Configuration No. 3		Configuration No. 4	
AXIAL POSITION	RADIUS	AXIAL POSITION	RADIUS	AXIAL POSITION	RADIUS	AXIAL POSITION	RADIUS
0.60960	0.12387	0.60960	0.12387	0.60960	0.12387	0.60960	0.12387
0.62230	0.12425	0.62230	0.12425	0.62230	0.12425	0.62230	0.12425
0.63500	0.12458	0.63500	0.12458	0.63500	0.12458	0.63500	0.12458
0.64770	0.12486	0.64770	0.12486	0.64770	0.12486	0.64770	0.12486
0.66040	0.12506	0.66040	0.12506	0.66040	0.12506	0.66040	0.12506
0.67310	0.12518	0.67310	0.12518	0.67310	0.12518	0.67310	0.12518
0.68580	0.12523	0.68580	0.12523	0.68580	0.12523	0.68580	0.12523
0.69850	0.12524	0.69850	0.12524	0.69850	0.12524	0.69850	0.12524
0.71120	0.12525	0.71120	0.12525	0.71120	0.12525	0.71120	0.12525
0.81280	0.12522	0.81280	0.12522	0.81280	0.12522	0.81280	0.12522
0.91440	0.12523	0.91440	0.12523	0.91440	0.12523	0.91440	0.12523
0.96393	0.12523	0.96393	0.12523	0.96393	0.12523	0.96393	0.12523
1.01600	0.12522	1.01600	0.12522	1.01600	0.12522	1.01600	0.12522
1.11760	0.12529	1.11760	0.12529	1.11760	0.12529	1.11760	0.12529
1.21920	0.12534	1.21920	0.12534	1.21920	0.12534	1.21920	0.12534
1.32080	0.12537	1.32080	0.12537	1.32080	0.12537	1.32080	0.12537
1.42240	0.12537	1.42240	0.12537	1.42240	0.12537	1.42240	0.12537
1.52400	0.12535	1.52400	0.12535	1.52400	0.12535	1.52400	0.12535
1.62560	0.12531	1.62560	0.12531	1.62560	0.12531	1.62560	0.12531
1.72720	0.12531	1.72720	0.12531	1.72720	0.12531	1.72720	0.12531
1.82880	0.12524	1.82880	0.12524	1.82880	0.12524	1.82880	0.12524
1.93040	0.12531	1.93040	0.12531	1.93040	0.12531	1.93040	0.12531
2.03200	0.12536	2.03200	0.12536	2.03200	0.12536	2.03200	0.12536
2.13360	0.12534	2.13360	0.12534	2.13360	0.12534	2.13360	0.12534
2.23520	0.12531	2.23520	0.12531	2.23520	0.12531	2.23520	0.12531
2.33680	0.12518	2.33680	0.12518	2.33680	0.12518	2.33680	0.12518
2.43840	0.12522	2.43840	0.12522	2.43840	0.12522	2.43840	0.12522
2.54000	0.12525	2.54000	0.12525	2.54000	0.12525	2.54000	0.12525
2.64160	0.12522	2.64160	0.12522	2.64160	0.12522	2.64160	0.12522
2.74320	0.12537	2.74320	0.12537	2.74320	0.12537	2.74320	0.12537
2.84480	0.12518	2.84480	0.12518	2.84480	0.12518	2.84480	0.12518
2.94640	0.12513	2.94640	0.12513	2.94640	0.12513	2.94640	0.12513
3.04800	0.12513	3.04800	0.12513	3.04800	0.12513	3.04800	0.12513
3.14960	0.12527	3.14960	0.12527	3.14960	0.12527	3.14960	0.12527
3.25120	0.12535	3.25120	0.12535	3.25120	0.12535	3.25120	0.12535
3.31394	0.12511	3.31394	0.12511	3.31394	0.12517	3.31394	0.12517
3.31711	0.12516	3.31711	0.12516	3.31711	0.12519	3.31711	0.12519
3.32029	0.12516	3.32029	0.12516	3.32029	0.12515	3.32029	0.12515
3.32346	0.12517	3.32346	0.12517	3.32346	0.12508	3.32346	0.12508
3.32664	0.12516	3.32664	0.12516	3.32664	0.12500	3.32664	0.12500
3.32981	0.12513	3.32981	0.12513	3.32981	0.12487	3.32981	0.12487
3.33299	0.12509	3.33299	0.12509	3.33299	0.12472	3.33299	0.12472
3.33616	0.12505	3.33616	0.12505	3.33616	0.12453	3.33616	0.12453
3.33934	0.12500	3.33934	0.12500	3.33934	0.12431	3.33934	0.12431
3.34251	0.12494	3.34251	0.12494	3.34251	0.12406	3.34251	0.12406
3.34569	0.12487	3.34569	0.12487	3.34569	0.12380	3.34569	0.12380

Table 1. Continued

Axial Position = MS, metric Local Model Radius = r, meters

Configuration No. 1		Configuration No. 2		Configuration No. 3		Configuration No. 4	
AXIAL POSITION	RADIUS	AXIAL POSITION	RADIUS	AXIAL POSITION	RADIUS	AXIAL POSITION	RADIUS
3.34886	0.12482	3.34886	0.12482	3.34886	0.12350	3.34886	0.12350
3.35204	0.12474	3.35204	0.12474	3.35204	0.12317	3.35204	0.12317
3.35521	0.12467	3.35521	0.12467	3.35521	0.12282	3.35521	0.12282
3.35839	0.12457	3.35839	0.12457	3.35839	0.12263	3.35839	0.12263
3.36156	0.12447	3.36156	0.12447	3.36156	0.12204	3.36156	0.12204
3.36474	0.12437	3.36474	0.12437	3.36474	0.12161	3.36474	0.12161
3.36791	0.12427	3.36791	0.12427	3.36791	0.12115	3.36791	0.12115
3.37109	0.12416	3.37109	0.12416	3.37109	0.12065	3.37109	0.12065
3.37426	0.12404	3.37426	0.12404	3.37426	0.12011	3.37426	0.12011
3.37744	0.12392	3.37744	0.12392	3.37744	0.11955	3.37744	0.11955
3.38061	0.12378	3.38061	0.12378	3.38061	0.11895	3.38061	0.11895
3.38379	0.12364	3.38379	0.12364	3.38379	0.11833	3.38379	0.11833
3.38696	0.12349	3.38696	0.12349	3.38696	0.11767	3.38696	0.11767
3.39014	0.12336	3.39014	0.12336	3.39014	0.11700	3.39014	0.11700
3.39331	0.12320	3.39331	0.12320	3.39331	0.11629	3.39331	0.11629
3.39649	0.12304	3.39649	0.12304	3.39649	0.11557	3.39649	0.11557
3.39966	0.12287	3.39966	0.12287	3.39966	0.11481	3.39966	0.11481
3.40284	0.12270	3.40284	0.12270	3.40284	0.11402	3.40284	0.11402
3.40601	0.12252	3.40601	0.12252	3.40601	0.11318	3.40601	0.11318
3.40919	0.12234	3.40919	0.12234	3.40919	0.11232	3.40919	0.11232
3.41236	0.12214	3.41236	0.12214	3.41236	0.11174	3.41236	0.11174
3.41554	0.12195	3.41554	0.12195	3.41554	0.11050	3.41554	0.11050
3.41871	0.12173	3.41871	0.12173	3.41871	0.10955	3.41871	0.10955
3.42189	0.12152	3.42189	0.12152	3.42189	0.10856	3.42189	0.10856
3.42506	0.12130	3.42506	0.12130	3.42506	0.10753	3.42506	0.10753
3.42824	0.12107	3.42824	0.12107	3.42824	0.10647	3.42824	0.10647
3.43141	0.12084	3.43141	0.12084	3.43141	0.10538	3.43141	0.10538
3.43459	0.12061	3.43459	0.12061	3.43459	0.10425	3.43459	0.10425
3.43776	0.12037	3.43776	0.12037	3.43776	0.10311	3.43776	0.10311
3.44094	0.12012	3.44094	0.12012	3.44094	0.10193	3.44094	0.10193
3.44411	0.11986	3.44411	0.11986	3.44411	0.10071	3.44411	0.10071
3.44729	0.11960	3.44729	0.11960	3.44729	0.09946	3.44729	0.09946
3.45046	0.11934	3.45046	0.11934	3.45046	0.09815	3.45046	0.09815
3.45364	0.11906	3.45364	0.11906	3.45364	0.09682	3.45364	0.09682
3.45681	0.11878	3.45681	0.11878	3.45681	0.09546	3.45681	0.09546
3.45999	0.11849	3.45999	0.11849	3.45999	0.09404	3.45999	0.09404
3.46316	0.11820	3.46316	0.11820	3.46316	0.09261	3.46316	0.09261
3.46634	0.11790	3.46634	0.11790	3.46634	0.09115	3.46634	0.09115
3.46951	0.11760	3.46951	0.11760	3.46951	0.08964	3.46951	0.08964
3.47269	0.11729	3.47269	0.11729	3.47269	0.08807	3.47269	0.08807
3.47586	0.11696	3.47586	0.11696	3.47586	0.08647	3.47586	0.08647
3.47904	0.11664	3.47904	0.11664	3.47904	0.08484	3.47904	0.08484
3.48221	0.11631	3.48221	0.11631	3.48221	0.08317	3.48221	0.08317
3.48539	0.11597	3.48539	0.11597	3.48539	0.08147	3.48539	0.08147
3.48856	0.11563	3.48856	0.11563	3.48856	0.07969	3.48856	0.07969
3.49174	0.11528	3.49174	0.11528	3.49174	0.07790	3.49174	0.07790

Table 1. Continued

Axial Position = MS, metric Local Model Radius = r, meters

Configuration No. 1		Configuration No. 2		Configuration No. 3		Configuration No. 4	
AXIAL POSITION	RADIUS	AXIAL POSITION	RADIUS	AXIAL POSITION	RADIUS	AXIAL POSITION	RADIUS
3.49491	0.11492	3.49491	0.11492	3.49491	0.07607	3.49491	0.07607
3.49809	0.11456	3.49809	0.11456	3.49809	0.07418	3.49809	0.07418
3.50126	0.11418	3.50126	0.11418	3.50126	0.07224	3.50126	0.07224
3.50444	0.11382	3.50444	0.11382	3.50444	0.07026	3.50444	0.07026
3.50761	0.11344	3.50761	0.11344	3.50761	0.06824	3.50761	0.06824
3.51079	0.11304	3.51079	0.11304	3.51079	0.06616	3.51079	0.06616
3.51396	0.11264	3.51396	0.11264	3.51429	0.06380	3.51429	0.06380
3.51714	0.11224	3.51714	0.11224	3.51434	0.06376	3.51434	0.06377
3.52031	0.11181	3.52031	0.11181	3.56514	0.06369	3.51752	0.06478
3.52349	0.11137	3.52349	0.11137	3.61594	0.06365	3.52069	0.06575
3.52666	0.11092	3.52666	0.11092	3.66674	0.06367	3.52387	0.06670
3.52984	0.11047	3.52984	0.11047	3.71754	0.06370	3.52704	0.06761
3.53301	0.11002	3.53301	0.11002	3.76834	0.06368	3.53022	0.06851
3.53116	0.10956	3.53116	0.10956	3.81914	0.06372	3.53339	0.06935
3.53936	0.10911	3.53936	0.10911	3.86994	0.06366	3.53657	0.07018
3.54254	0.10866	3.54254	0.10866	3.92074	0.06361	3.53974	0.07097
3.54571	0.10820	3.54571	0.10820	3.97154	0.06358	3.54292	0.07173
3.54889	0.10774	3.54889	0.10774	4.02234	0.06360	3.54609	0.07247
3.55206	0.10728	3.55206	0.10728	4.07314	0.06358	3.54927	0.07319
3.55524	0.10683	3.55524	0.10683	4.12394	0.06357	3.55244	0.07388
3.55841	0.10635	3.55841	0.10635	4.17474	0.06356	3.55562	0.07455
3.56159	0.10585	3.56159	0.10585	4.22554	0.06354	3.55879	0.07519
3.56476	0.10536	3.56476	0.10536	4.27634	0.06360	3.56197	0.07582
3.56794	0.10486	3.56794	0.10486	4.32714	0.06365	3.56514	0.07642
3.57111	0.10436	3.57111	0.10436	4.37794	0.06370	3.56832	0.07698
3.57429	0.10385	3.57429	0.10385	4.42874	0.06375	3.57149	0.07752
3.57746	0.10332	3.57746	0.10332	4.47954	0.06374	3.57467	0.07804
3.58064	0.10280	3.58064	0.10280	4.53034	0.06369	3.57784	0.07855
3.58381	0.10227	3.58381	0.10227	4.58114	0.06360	3.58102	0.07903
3.58699	0.10173	3.58699	0.10173	4.63194	0.06351	3.58419	0.07948
3.59016	0.10118	3.59016	0.10118			3.58737	0.07994
3.59334	0.10062	3.59334	0.10062			3.59054	0.08039
3.59651	0.10005	3.59651	0.10005			3.59372	0.08079
3.59969	0.09949	3.59969	0.09949			3.59689	0.08118
3.60286	0.09892	3.60286	0.09892			3.60007	0.08154
3.60604	0.09835	3.60604	0.09835			3.60324	0.08189
3.60921	0.09776	3.60921	0.09776			3.60642	0.08230
3.61239	0.09718	3.61239	0.09718			3.60959	0.08253
3.61556	0.09658	3.61556	0.09658			3.61277	0.08282
3.61874	0.09597	3.61874	0.09597			3.61594	0.08310
3.62191	0.09535	3.62191	0.09535			3.61912	0.08335
3.62509	0.09474	3.62509	0.09474			3.62229	0.08359
3.62826	0.09412	3.62826	0.09412			3.62547	0.08381
3.63144	0.09348	3.63144	0.09348			3.62864	0.08402
3.63461	0.09283	3.63461	0.09283			3.63182	0.08421
3.63779	0.09219	3.63779	0.09219			3.63499	0.08439

Table 1. Continued

Axial Position = MS, metric Local Model Radius = r, meters

Configuration No. 1		Configuration No. 2		Configuration No. 3		Configuration No. 4	
AXIAL POSITION	RADIUS	AXIAL POSITION	RADIUS	AXIAL POSITION	RADIUS	AXIAL POSITION	RADIUS
3.64096	0.09153	3.64096	0.09153			3.63817	0.08472
3.64414	0.09088	3.64414	0.09088			3.64134	0.08470
3.64731	0.09022	3.64731	0.09022			3.64452	0.08483
3.65049	0.08956	3.65049	0.08956			3.64769	0.08492
3.65366	0.08889	3.65366	0.08889			3.65087	0.08502
3.65684	0.08821	3.65684	0.08821			3.65404	0.08508
3.66001	0.08752	3.66001	0.08752			3.65722	0.08511
3.66319	0.08682	3.66319	0.08682			3.66039	0.08512
3.66636	0.08612	3.66636	0.08612			3.66357	0.08512
3.66954	0.08542	3.66954	0.08542			3.66674	0.08575
3.67271	0.08469	3.67271	0.08469			3.67175	0.08508
3.67589	0.08397	3.67589	0.08397				
3.67906	0.08325	3.67906	0.08325				
3.68224	0.08252	3.68224	0.08252				
3.68541	0.08177	3.68541	0.08177				
3.68859	0.08102	3.68859	0.08102				
3.69176	0.08025	3.69176	0.08025				
3.69494	0.07949	3.69494	0.07949				
3.69811	0.07873	3.69811	0.07873				
3.70129	0.07797	3.70129	0.07797				
3.70446	0.07718	3.70446	0.07718				
3.70764	0.07639	3.70764	0.07639				
3.71081	0.07559	3.71081	0.07559				
3.71399	0.07478	3.71399	0.07478				
3.71716	0.07396	3.71716	0.07396				
3.72034	0.07315	3.72034	0.07315				
3.72351	0.07233	3.72351	0.07233				
3.72669	0.07150	3.72669	0.07150				
3.72986	0.07066	3.72986	0.07066				
3.73304	0.06982	3.73304	0.06982				
3.73621	0.06898	3.73621	0.06898				
3.73939	0.06812	3.73939	0.06812				
3.74256	0.06726	3.74256	0.06726				
3.74574	0.06640	3.74574	0.06640				
3.74891	0.06551	3.74891	0.06551				
3.75209	0.06464	3.75209	0.06464				
3.75526	0.06363	3.75526	0.06363				
3.75671	0.06376	3.75671	0.06377				
3.80751	0.06369	3.75988	0.06478				
3.85831	0.06365	3.76306	0.06575				
3.90911	0.06367	3.76623	0.06670				
3.95991	0.06370	3.76941	0.06761				
4.01071	0.06368	3.77258	0.06851				
4.06151	0.06372	3.77576	0.06935				
4.11231	0.06366	3.77893	0.07018				
4.16311	0.06361	3.78211	0.07097				

Table 1. Concluded

Axial Position = MS, metric Local Model Radius = r, meters

Configuration No. 1		Configuration No. 2		Configuration No. 3		Configuration No. 4	
AXIAL POSITION	RADIUS	AXIAL POSITION	RADIUS	AXIAL POSITION	RADIUS	AXIAL POSITION	RADIUS
4.21391	0.06358	3.78528	0.07173				
4.26471	0.06360	3.78846	0.07247				
4.31551	0.06358	3.79163	0.07319				
4.36631	0.06357	3.79481	0.07388				
4.41711	0.06356	3.79799	0.07455				
4.46791	0.06354	3.80116	0.07519				
4.51871	0.06360	3.80433	0.07582				
4.56951	0.06365	3.80751	0.07642				
4.62031	0.06370	3.81132	0.07698				
4.67111	0.06375	3.81386	0.07752				
4.72191	0.06374	3.81703	0.07804				
4.77271	0.06369	3.82021	0.07855				
4.82351	0.06360	3.82339	0.07903				
4.87431	0.06351	3.82656	0.07948				
		3.82973	0.07994				
		3.83291	0.08039				
		3.83608	0.08079				
		3.83926	0.08118				
		3.84243	0.08154				
		3.84561	0.08189				
		3.84878	0.08230				
		3.85196	0.08253				
		3.85513	0.08282				
		3.85831	0.08310				
		3.86148	0.08335				
		3.86466	0.08359				
		3.86784	0.08381				
		3.87101	0.08402				
		3.87418	0.08421				
		3.87736	0.08439				
		3.88054	0.08472				
		3.88371	0.08470				
		3.88688	0.08483				
		3.89006	0.08492				
		3.89324	0.08502				
		3.89641	0.08508				
		3.89958	0.08511				
		3.90276	0.08512				
		3.90593	0.08512				
		3.90911	0.08575				
		3.91411	0.08508				

Table 2. Test Matrix

M_∞	Unit Reynolds Number (m^{-1}) x 10^{-6}			
	3.28	8.20	11.48	13.12
0.6	3[2];4 S[2] S	1, 2, ③[3], 4 S S S T T T		1, 2, 3, 4 S S S S T
0.7	3, 4 S S	1, 3, 4 S S S T T T		3, 4 S S T T
0.8	1, 3, 4 S S S T	①, 2, 3, 4 S S S T T		1, 2, 3, 4 S S S S T
0.85		1, 2, 3, 4 S S S T T		1, 2, 3, 4 S S S S T
0.90		1, 2, 3, 4 S S S T T		1, 2, 3, 4 S S S S T
0.95		1, 2, ③, 4 S S S T T		1, 2, 3, 4 S S S S T T
1.10		1, 2, 3, 4 S S S T T		1, 2, 3, 4 S S S S T
1.20		1, 2, 3, 4 S S S T T	1, 2, 3, 4 S S S S T	
1.30		1, 2, 3, 4 S S S T	1, 2, 3, 4 S S S S T	

[1]Pressure distributions and boundary-layer pitot data available on all test points.

[2]Model configuration (see Fig. 6). S indicates schlieren data available. T indicates tuft data available.

[3]Circle indicates data presented in this report.

Table 3. Measurement Uncertainties

Parameter	Uncertainty, Ui							
	Re_∞ = 3.3 x 10^6 m^{-1} (1 x 10^6 ft^{-1})		Re_∞ = 8.2 x 10^6 m^{-1} (2.5 x 10^6 ft^{-1})		Re_∞ = 11.48 x 10^6 m^{-1} (3.5 x 10^6 ft^{-1})	Re_∞ = 13.12 x 10^6 m^{-1}) (4 x 10^6 ft^{-1})		
	M_∞ = 0.6	M_∞ = 0.8	M_∞ = 0.95	M_∞ = 1.3	M_∞ = 1.3	M_∞ = 0.6	M_∞ = 0.8	M_∞ = 0.95
M_∞	±0.0134	±0.0106	±0.00387	±0.00335	±0.00312	±0.0037	±0.0028	±0.00232
PT, pascals, psfa	$\pm^{113.8}_{(2.376)}$	$\pm^{113.1}_{(2.363)}$	$\pm^{117.1}_{(2.446)}$	$\pm^{116.9}_{(2.441)}$	$\pm^{119.6}_{(2.497)}$	$\pm^{124.4}_{(2.599)}$	$\pm^{122.1}_{(2.551)}$	$\pm^{121.3}_{(2.534)}$
P_∞, pascals, psfa	$\pm^{263.72}_{(5.508)}$	$\pm^{188.0}_{(3.926)}$	$\pm^{156.90}_{(3.277)}$	$\pm^{104.0}_{(2.171)}$	$\pm^{130.0}_{(2.714)}$	$\pm^{289.1}_{(6.037)}$	$\pm^{199.5}_{(4.167)}$	$\pm^{152.8}_{(3.191)}$
q_∞, pascals, psfa	$\pm^{494.22}_{(10.322)}$	$\pm^{153.4}_{(3.204)}$	$\pm^{116.2}_{(2.428)}$	$\pm^{60.3}_{(1.258)}$	$\pm^{62.7}_{(1.310)}$	$\pm^{330.0}_{(6.892)}$	$\pm^{162.7}_{(3.399)}$	$\pm^{116.3}_{(2.429)}$
CP* = 0	±0.0542	±0.0345	±0.0126	±0.0086	±0.0070	±0.0190	±0.01166	±0.0089

*These values represent the rms expected error in CP = 0.

Table 4. Tabulated Data
NOMENCLATURE

CP	Static pressure coefficient
M_∞	Free-stream Mach number
Re_∞	Unit Reynolds number, m^{-1}
PT	Total-pressure, pascals
TS	Free-stream static pressure, °K
Y	Boundary-layer coordinate normal to model surface, m
Axial Position	Distance from model tip equal to MS - 0.0183, m
PART	Data index number
PS	Static pressure at the boundary-layer rake position, pascals

Table 4. Tabulated Data

Configuration No. 1

Part 1023

M_∞ = 0.798

$Re_\infty \times 10^{-6}$ = 8.190

PT = 62746.7

TS = 305.4

Axial Position	CP
0.05080	0.2750
0.07620	0.2599
0.10160	0.2446
0.12700	0.2202
0.15240	0.2012
0.17780	0.1854
0.20320	0.1615
0.22860	0.1638
0.25400	0.1514
0.27940	0.1400
0.33020	0.0593
0.35560	0.0173
0.38100	-0.0495
0.40640	-0.1317
0.43180	-0.1824
0.45720	-0.2050
0.48260	-0.2208
0.50800	-0.2141
0.53340	-0.2369
0.60960	-0.1587
0.63500	-0.1493
0.66040	-0.1451
0.68580	-0.0988
0.71120	-0.0786
0.73660	-0.0637
0.76200	-0.0537
0.78740	-0.0487
0.81280	-0.0421
0.83820	-0.0385
0.86360	-0.0353
0.88900	-0.0312
0.91440	-0.0301
0.93980	-0.0237
1.04140	-0.0237

Configuration No. 3

Part 1074

M_∞ = 0.599

$Re_\infty \times 10^{-6}$ = 8.224

PT = 75200.3

TS = 306.0

Axial Position	CP
0.05080	0.2373
0.07620	0.2321
0.10160	0.2161
0.12700	0.1902
0.15240	0.1730
0.17780	0.1574
0.20320	0.1333
0.22860	0.1368
0.25400	0.1245
0.27940	0.1124
0.33020	0.0400
0.35560	0.0034
0.38100	-0.0533
0.40640	-0.1159
0.43180	-0.1550
0.45720	-0.1706
0.48260	-0.1810
0.50800	-0.1759
0.53340	-0.1972
0.60960	-0.1368
0.63500	-0.1309
0.66040	-0.1253
0.68580	-0.0866
0.71120	-0.0727
0.73660	-0.0579
0.76200	-0.0501
0.78740	-0.0465
0.81280	-0.0402
0.83820	-0.0374
0.86360	-0.0355
0.88900	-0.0307
0.91440	-0.0285
0.93980	-0.0181
1.04140	-0.0286

Part 1083

M_∞ = 0.948

Re_∞ = 10^{-6} = 8.099

PT = 57637.9

TS = 304.9

CP
0.3285
0.3189
0.3075
0.2759
0.2555
0.2413
0.2181
0.2219
0.2150
0.2080
0.1223
0.0782
0.0051
-0.1032
-0.1816
-0.2335
-0.2787
-0.3177
-0.3090
-0.3567
-0.3430
-0.3453
-0.2684
-0.0535
-0.0056
0.0006
-0.0025
-0.0039
-0.0061
-0.0091
-0.0072
-0.0063
0.0042
-0.0201

Table 4. Continued

Configuration No. 1

Part 1023

M_∞ = 0.798

$Re_\infty \times 10^{-6}$ = 8.190

PT = 62746.7

TS = 305.4

Axial Position	CP
1.06680	-0.0236
1.09220	-0.0220
1.11760	-0.0189
1.14300	-0.0175
1.16840	-0.0189
1.19380	-0.0148
1.21920	-0.0202
1.24460	-0.0126
1.27000	-0.0162
1.42240	-0.0128
1.57480	-0.0101
1.72720	-0.0123
1.87960	-0.0306
2.03200	-0.0094
2.18440	-0.0116
2.33680	0.0167
2.48920	-0.0072
2.64160	-0.0105
2.79400	-0.0210
2.80670	-0.0184
2.81940	-0.0131
2.83210	-0.0137
2.84480	-0.0098
2.85750	-0.0204
2.87020	-0.0200
2.88290	-0.0147
2.89560	-0.0209
2.90830	-0.0221
2.92100	-0.0212
2.93370	-0.0190
2.94640	-0.0233
2.95910	-0.0211
2.97180	-0.0228
2.98450	-0.0199
2.99720	-0.0220
3.00990	-0.0260
3.02260	-0.0257
3.03530	-0.0235
3.04800	-0.0271
3.06070	-0.0278

Configuration No. 3

Part 1074

M_∞ = 0.599

$Re_\infty \times 10^{-6}$ = 8.224

PT = 75200.3

TS = 306.0

Axial Position	CP
1.06680	-0.0278
1.09220	-0.0229
1.11760	-0.0235
1.14300	-0.0176
1.16840	-0.0191
1.19380	-0.0150
1.21920	-0.0177
1.24460	-0.0129
1.27000	-0.0162
1.42240	-0.0127
1.57480	-0.0107
1.72720	-0.0110
1.87960	-0.0086
2.03200	-0.0101
2.18440	-0.0113
2.33680	0.0140
2.48920	-0.0076
2.64160	-0.0106
2.79400	-0.0194
2.80670	-0.0162
2.81940	-0.0149
2.83210	-0.0177
2.84480	-0.0131
2.85750	-0.0240
2.87020	-0.0222
2.88290	-0.0185
2.89560	-0.0246
2.90830	-0.0259
2.92100	-0.0256
2.93370	-0.0242
2.94640	-0.0279
2.95910	-0.0271
2.97180	-0.0353
2.98450	-0.0273
2.99720	-0.0306
3.00990	-0.0336
3.02260	-0.0344
3.03530	-0.0320
3.04800	-0.0384
3.06070	-0.0380

Part 1083

M_∞ = 0.948

Re_∞ = 10^{-6} = 8.099

PT = 57637.9

TS = 304.9

CP
-0.0202
-0.0164
-0.0170
-0.0124
-0.0143
-0.0109
-0.0139
-0.0094
-0.0099
-0.0080
-0.0063
-0.0077
-0.0059
-0.0085
-0.0095
0.0252
-0.0043
-0.0081
-0.0149
-0.0114
-0.0101
-0.0118
-0.0091
-0.0198
-0.0188
-0.0163
-0.0223
-0.0236
-0.0241
-0.0224
-0.0256
-0.0242
-0.0243
-0.0197
-0.0222
-0.0253
-0.0259
-0.0238
-0.0287
-0.0285

Table 4. Continued

Configuration No. 1

Part 1023

M_∞ = 0.798

$Re_\infty \times 10^{-6}$ = 8.190

PT = 62746.7

TS = 305.4

Axial Position	CP
3.07340	-0.0259
3.08610	-0.0315
3.09880	-0.0309
3.11150	-0.0311
3.12420	-0.0351
3.13690	-0.0331
3.14960	-0.0329
3.16230	-0.0425
3.17500	-0.0438
3.18770	-0.0367
3.20040	-0.0485
3.21310	-0.0576
3.22580	-0.0560
3.23850	-0.0626
3.25120	-0.0870
3.26390	-0.0821
3.27660	-0.0586
3.32664	-0.1713
3.33934	-0.1576
3.35204	-0.1615
3.36474	-0.1485
3.37744	-0.1596
3.39014	-0.1552
3.40284	-0.1631
3.41554	-0.1576
3.42824	-0.1482
3.44094	-0.1463
3.45364	-0.1597
3.46634	-0.1367
3.47904	-0.1260
3.49174	-0.1212
3.50444	-0.1198
3.51714	-0.1130
3.52984	-0.0943
3.54254	-0.0740
3.55524	-0.0712
3.56794	-0.0596
3.58064	-0.0512

Configuration No. 3

Part 1074

M_∞ = 0.599

$Re_\infty \times 10^{-6}$ = 8.224

PT = 75200.3

TS = 306.0

Axial Position	CP
3.07340	-0.0368
3.08610	-0.0425
3.09880	-0.0425
3.11150	-0.0440
3.12420	-0.0493
3.13690	-0.0483
3.14960	-0.0467
3.16230	-0.0582
3.17500	-0.0616
3.18770	-0.0546
3.20040	-0.0710
3.21310	-0.0814
3.22580	-0.0845
3.23850	-0.0934
3.25120	-0.1234
3.26390	-0.1260
3.27660	-0.1089
3.32664	-0.2984
3.33934	-0.3092
3.35204	-0.3049
3.36474	-0.3042
3.37744	-0.2724
3.39014	-0.2236
3.40284	-0.1822
3.41554	-0.1164
3.42824	-0.0499
3.44094	0.0200
3.45364	0.0701
3.46634	0.0970
3.47904	0.1068
3.49174	0.1116
3.50444	0.1116
3.52044	0.1187
3.53314	0.1397
3.54584	0.1624
3.55854	0.1781
3.57124	0.1854
3.58394	0.1870

Part 1083

M_∞ = 0.948

Re_∞ = 10^{-6} = 8.099

PT = 57637.9

TS = 304.9

CP
-0.0264
-0.0329
-0.0320
-0.0332
-0.0379
-0.0355
-0.0328
-0.0438
-0.0462
-0.0408
-0.0546
-0.0630
-0.0653
-0.0730
-0.0995
-0.1022
-0.0824
-0.3638
-0.4369
-0.5022
-0.5668
-0.3716
-0.1708
-0.1001
-0.0748
-0.0591
-0.0510
-0.0466
-0.0420
-0.0430
-0.0447
-0.0449
-0.0419
-0.0371
-0.0183
0.0023
0.0265
0.0498

Table 4. Continued

Configuration No. 1

Part 1023

M_∞ = 0.798

$Re_\infty \times 10^{-6}$ = 8.190

PT = 62746.7

TS = 305.4

Axial Position	CP
3.59334	-0.0332
3.60604	-0.0188
3.61874	-0.0011
3.63144	0.0153
3.64414	0.0350
3.65684	0.0520
3.66954	0.0693
3.68224	0.0917
3.69494	0.1137
3.70764	0.1350
3.72034	0.1590
3.73304	0.1826
3.74574	0.2063
3.76306	0.2217
3.77576	0.2047
3.78846	0.1860
3.80116	0.1691
3.81386	0.1541
3.82656	0.1405
3.83926	0.1284
3.85196	0.1207
3.86466	0.1072
3.87736	0.0990
3.89006	0.0904
3.90276	0.0806
3.91546	0.0772
3.92816	0.0707
3.94086	0.0661
3.95356	0.0617
3.96626	0.0573
3.97896	0.0519
3.99166	0.0559
4.00436	0.0472
4.01706	0.0451
4.02976	0.0403
4.04246	0.0379
4.05516	0.0355
4.06786	0.0345
4.08056	0.0321
4.09326	0.0292

Configuration No. 3

Part 1074

M_∞ = 0.599

$Re_\infty \times 10^{-6}$ = 8.224

PT = 75200.3

TS = 306.0

Axial Position	CP
3.59664	0.1822
3.60934	0.1726
3.62204	0.1568
3.63474	0.1464
3.64744	0.1344
3.66014	0.1232
3.67284	0.1143
3.68554	0.1038
3.69824	0.0959
3.71094	0.0879
3.72364	0.0801
3.73634	0.0716
3.74904	0.0717
3.76174	0.0620
3.77444	0.0574
3.78714	0.0510
3.79984	0.0491
3.81254	0.0427
3.82524	0.0408
3.83794	0.0370
3.85064	0.0334
3.86334	0.0320
3.87604	0.0274
3.88874	0.0269
3.90144	0.0246
3.91414	0.0215
3.92684	0.0216
3.93954	0.0195
3.95224	0.0170
3.96494	0.0197
3.97764	0.0158
3.99034	0.0144
4.00304	0.0127
4.01574	0.0129
4.02844	0.0130
4.04114	0.0128
4.05384	0.0122
4.07924	0.0113
4.10464	0.0106
4.13004	0.0087

Part 1083

M_∞ = 0.948

$Re_\infty = 10^{-6}$ = 8.099

PT = 57637.9

TS = 304.9

CP
0.0770
0.1008
0.1134
0.1307
0.1454
0.1523
0.1532
0.1538
0.1566
0.1518
0.1462
0.1413
0.1396
0.1321
0.1285
0.1196
0.1140
0.1066
0.1021
0.0954
0.0891
0.0847
0.0772
0.0738
0.0697
0.0643
0.0619
0.0579
0.0545
0.0545
0.0485
0.0458
0.0429
0.0414
0.0389
0.0364
0.0342
0.0305
0.0289
0.0252

Table 4. Continued

Configuration No. 1

Part 1023

M_∞ = 0.798

$Re_\infty \times 10^{-6}$ = 8.190

PT = 62746.7

TS = 305.4

Axial Position	CP
4.10596	0.0296
4.11866	0.0250
4.13136	0.0269
4.14406	0.0267
4.15676	0.0242
4.16946	0.0242
4.18216	0.0244
4.19486	0.0237
4.20756	0.0266
4.22026	0.0239
4.23296	0.0222
4.24566	0.0215
4.25836	0.0218
4.27106	0.0203
4.28376	0.0181
4.29646	0.0197
4.32186	0.0166
4.34726	0.0203
4.37266	0.0196
4.39806	0.0174
4.42346	0.0187
4.44886	0.0197
4.47426	0.0191
4.49966	0.0227
4.52506	0.0202
4.55046	0.0235
4.57586	0.0321
4.60126	0.0303
4.62666	0.0289
4.65206	0.0310
4.67746	0.0362
4.70286	0.0509
4.72826	0.0525
4.75366	0.0551
4.77906	0.0576
4.80446	0.0590
4.82986	0.0601
4.85526	0.0608
4.88066	0.1304
4.90606	0.1303

Configuration No. 3

Part 1074

M_∞ = 0.599

$Re_\infty \times 10^{-6}$ = 8.224

PT = 75200.3

TS = 306.0

Axial Position	CP
4.15544	0.0062
4.18084	0.0052
4.20624	0.0063
4.23164	0.0029
4.25704	0.0065
4.28244	0.0010
4.30784	0.0028
4.33324	0.0034
4.35864	0.0052
4.38404	0.0003
4.40944	-0.0003
4.43484	-0.0024
4.46024	-0.0020
4.48564	0.0013
4.51104	0.0033
4.53644	0.0008
4.56184	0.0042
4.58724	0.0013
4.61264	0.0000
4.63804	0.0056
4.66344	0.0053

Part 1083

M_∞ = 0.948

$Re_\infty = 10^{-6}$ = 8.099

PT = 57637.9

TS = 304.9

CP
0.0204
0.0194
0.0196
0.0165
0.0195
0.0134
0.0147
0.0167
0.0183
0.0128
0.0132
0.0115
0.0125
0.0174
0.0209
0.0195
0.0250
0.0234
0.0245
0.0334
0.0386

Table 4. Continued

Configuration No. 1

Part 1023

M_∞ = 0.798

$Re_\infty \times 10^{-6}$ = 8.190

PT = 62746.7

TS = 305.4

BOUNDARY-LAYER RAKE AXIAL POSITION = 2.8824

Y	PT101
0.00038	47480.5
0.00483	52387.2
0.00991	54757.7
0.01549	57056.0
0.02134	59358.8
0.02794	61267.5
0.03556	62475.8
0.04420	62672.8
0.05385	62396.9
0.06350	62698.9
	PS = 37885.2

BOUNDARY-LAYER RAKE AXIAL POSITION = 3.5982

Y	PT211
0.00140	47020.4
0.00686	52312.5
0.01422	55177.7
0.02184	57389.9
0.03048	59637.0
0.03962	61523.8
0.05004	62552.0
0.06198	62716.8
0.07518	62747.1
0.08966	62708.1
	PS = 40629.0

BOUNDARY-LAYER RAKE AXIAL POSITION = 3.7567

Y	PT311
0.00140	46515.5
0.01067	50102.0
0.02032	53289.0
0.03048	56106.1
0.04318	58706.4
0.05690	61136.1
0.07214	62607.0
0.08890	62790.9
0.10770	62799.6
0.12852	62804.0
	PS = 40298.0

Configuration No. 3

Part 1074

M_∞ = 0.599

$Re_\infty \times 10^{-6}$ = 8.224

PT = 75200.3

TS = 306.0

BOUNDARY-LAYER RAKE AXIAL POSITION = 2.8824

Y	PT101
0.00038	64072.0
0.00483	67741.8
0.00991	69545.4
0.01549	71211.8
0.02134	72819.1
0.02794	74201.9
0.03556	74978.4
0.04420	75056.8
0.05385	74987.1
0.06350	75200.3
	PS = 56684.1

BOUNDARY-LAYER RAKE AXIAL POSITION = 3.4313

Y	PT201
0.00152	64135.0
0.00711	68164.8
0.01422	70224.8
0.02210	71799.9
0.03023	73203.9
0.03912	74550.8
0.05131	75037.8
0.06274	75099.2
0.07544	75099.2
0.08941	75112.4
	PS = 58243.3

BOUNDARY-LAYER RAKE AXIAL POSITION = 3.5194

Y	PT301
0.00610	60627.1
0.01524	61205.6
0.02476	64744.0
0.03480	68943.5
0.04775	71425.5
0.06198	73608.7
0.07671	74851.8
0.09373	75104.9
0.11278	75039.4
0.13310	75170.3
	PS = 60639.4

Part 1083

M_∞ = 0.948

$Re_\infty \times 10^{-6}$ = 8.099

PT = 57637.9

TS = 304.9

PT101
39482.0
44853.7
47760.6
50386.8
53022.0
55516.8
57266.2
57700.1
57559.9
57637.9
PS = 28641.7

PT201
30943.4
34533.4
44910.5
48518.4
51457.5
54299.8
56697.8
57370.9
57274.1
57234.5
PS = 31131.1

PT301
31192.9
31018.8
31304.0
33063.3
40493.3
49505.6
54885.4
57481.0
57467.8
57516.1
PS = 31419.7

Table 4. Concluded

Configuration No. 1

Part 1023

M_∞ = 0.798

$Re_\infty \times 10^{-6}$ = 8.190

PT = 62746.7

TS = 305.4

BOUNDARY-LAYER RAKE AXIAL POSITION = 3.8405

Y	PT411
0.00114	48324.6
0.00914	50795.9
0.01854	54035.4
0.02972	56762.7
0.04166	59021.6
0.05537	61390.1
0.07010	62650.9
0.08636	62790.9
0.10541	62760.2
0.12573	62755.9
PS =	43822.4

Configuration No. 3

Part 1074

M_∞ = 0.599

$Re_\infty \times 10^{-6}$ = 8.224

PT = 75200.3

TS = 306.0

BOUNDARY-LAYER RAKE AXIAL POSITION = 3.5982

Y	PT411
0.00114	63427.7
0.00914	64905.4
0.01854	67975.1
0.02972	70505.1
0.04166	72223.8
0.05537	73922.7
0.07010	75043.7
0.08636	75200.7
0.10541	75196.4
0.12573	75200.7
PS =	61758.6

Part 1083

M_∞ = 0.948

$Re_\infty \times 10^{-6}$ = 8.099

PT = 57637.9

TS = 304.9

PT411
34074.4
34088.1
35018.7
38417.3
44476.6
51044.6
55389.6
57603.8
57669.6
57625.7
PS = 33345.5

Table 5. Two-Dimensional Boundary-Layer Integral Parameters

Axial Position	Configuration No. 1 $M_\infty = 0.8$, $Re_\infty = 8.2 \times 10^6$/m				Axial Position	Configuration No. 3 $M_\infty = 0.6$, $Re_\infty = 8.2 \times 10^6$/m				$M_\infty = 0.95$, $Re_\infty = 8.2 \times 10^6$/m			
	δ^*	θ	c_f	R_θ		δ^*	θ	c_f	R_θ	δ^*	θ	c_f	R_θ
2.882	4.39^{-3}	2.76^{-3}	2.20^{-3}	2.351^{4}	2.882	4.343^{-3}	3.028^{-3}	2.25^{-3}	2.616^{4}	5.351^{-3}	3.129^{-3}	2.05^{-3}	2.636^{4}
3.598	6.98^{-3}	4.31^{-3}	2.00^{-3}	3.556^{4}	3.431	6.390^{-3}	4.337^{-3}	2.00^{-3}	3.580^{4}	S	S	S	S
3.757	1.190^{-2}	7.138^{-3}	1.55^{-3}	5.917^{4}	3.519	S**	S	S	S	S	S	S	S
3.840	1.264^{-2}	7.587^{-3}	1.45^{-3}	5.934^{4}	3.598	1.577^{-2}	8.837^{-3}	8.50^{-4}	6.684^{4}	S	S	S	S

* Axial position is distance from model tip = MS - 0.0183, m; all dimensions are in meters.

** S indicates that the profile is considered to be separated.

NOMENCLATURE

BTS	Boattail axial coordinate with origin at forebody boattail junction, cm
c_f	Local skin friction coefficient
CP	Pressure coefficient, $(PS - P_\infty)/q_\infty$
D	Model maximum diameter, 25.04 cm (9.86 in.)
ℓ	Length of boattail, cm
M_∞	Tunnel (free-stream) Mach number
MS	Model axial coordinate with origin 0.0183 m ahead of model nose (origin of conical section of model nose), cm or m
P_∞	Tunnel (free-stream) static pressure, pascals*
PS	Local static pressure, pascals
PT	Tunnel (free-stream) total pressure, pascals
q_∞	Tunnel (free-stream) dynamic pressure, $PS - M_\infty^2/2$
r	Local model radius, m
Re_∞	Unit Reynolds number, m^{-1}
R_θ	Reynolds number based on local boundary-layer edge conditions and momentum thickness

SPS	Solid plume axial coordinate with origin at boattail-plume junction, (cm)
TS	Tunnel (free-stream) static temperature
Ui	Uncertainty in parameter i
v	Velocity
v_e	Boundary-layer edge velocity
$\overline{X}$	Nondimensional boattail location (MS-331.29)/D
Y	Boundary-layer coordinate normal to model surface
δ^*	Two-dimensional displacement thickness, m $\int_o^\infty (1 - \rho v/\rho_e v_e) dY$
θ	Two-dimensional momentum thickness, m $\int_o^\infty (1 - v/v_e)\rho v/\rho_e v_e dY$
γ	Ratio of specific heats
ρ	Density
ρ_e	Boundary-layer edge density

*1 pascal = Newton/m^2